# Mandelstam diagrams are not enough to study the high-energy behavior of $\phi^3$ theory*

Barry M. McCoy†
*Institute for Theoretical Physics, State University of New York, Stony Brook, New York 11794*
Tai Tsun Wu‡
*Fermi National Accelerator Laboratory, Batavia, Illinois 60510§*
(Received 18 November 1974)

Viewed in the crossed channel, the $\phi^3$ Mandelstam diagrams for the Reggeon-particle cut represent repeated interaction between two of the three exchanged particles. A much larger class of Feynman diagrams is obtained by allowing all three exchanged particles to participate in the interaction, as required by Bose statistics. It is found that, in the limit of high energies, all diagrams of the same order in this larger class contribute comparably. In particular, the contributions from the Mandelstam and non-Mandelstam diagrams are of the same order of magnitude. This larger class of diagrams is summed in terms of an integral equation. It is found from this integral equation that if the momentum transfer is not too large, then the leading singularity in the angular momentum plane is a pole. As the momentum transfer increases this pole eventually disappears into a cut. These considerations are generalized, in a nontrivial way, to the case of the Reggeon-Reggeon cut. The signature factor plays a most important role, and some of the contributing diagrams show unexpected high-energy behavior. The profound effect of these additional diagrams on the program of Reggeon calculus is discussed.

## I. INTRODUCTION

In 1963, Mandelstam[1] invented his famous diagrams, shown in Fig. 1, that give the Reggeon-particle cut in $\phi^3$ theory. In the ensuing decade, many authors[2-20] have studied the properties of Regge cuts from various point of view.

Let us look at the Mandelstam diagrams of Fig. 1 from the crossed, or $t$, channel. We see three particles, two of which interact repeatedly with each other, while the third one participates only at the two ends. We recall, however, that in $\phi^3$ theory all the particles are the same. Thus the idea of emphasizing the Mandelstam diagrams, with their choice of interaction mainly between two of the three particles, seems inconsistent with the concept of *identical particles*.

It was Mandelstam himself who warned that at high energies there may be other diagrams which are just as important as those that he explicitly considered. In fact, Polkinghorne[3] subsequently produced such a diagram. However, the complete set of diagrams which, at high energies, are comparable to the Mandelstam diagrams has never been obtained. It is the purpose of this paper to present this complete set of diagrams and to study the properties of the resulting amplitude.

From the point of view of identical particles, this complete set of diagrams can be easily described. Aside from the technical problem of avoiding the pitfall of the AFS (Amati-Fubini-Stanghellini) diagrams,[21] the complete set of diagrams is obtained by permitting arbitrary orders of repeated pairwise interaction between the three exchanged particles. In this way, *the direct and exchange interactions are treated completely on the same footing*. Some examples of such diagrams are shown in Fig. 2. As $s \to \infty$ with fixed $t$, the

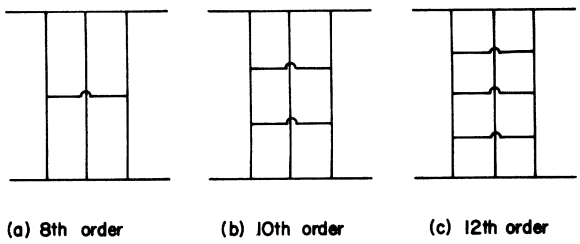


FIG. 1. The $\phi^3$ Feynman diagrams of Mandelstam. The $s$ channel runs horizontally from left to right, and the $t$ channel is vertical.

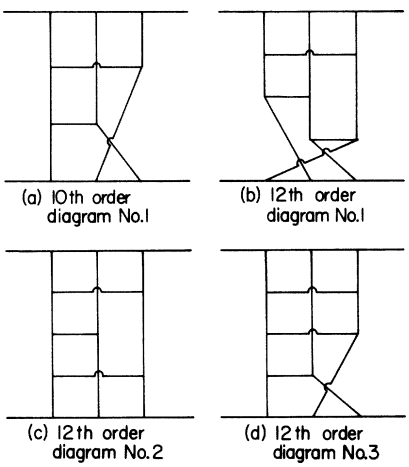


FIG. 2. Non-Mandelstam diagrams, which in $\phi^3$ are of comparable magnitude as the Mandelstam diagrams of the same order.

contribution from the diagram of Fig. 2(a) is of the same order of magnitude as that of the diagram of Fig. 1(b), while those from Figs. 2(b), 2(c), and 2(d) are of the same magnitude as that of Fig. 1(c). More generally, the contribution from any diagram of this class is of the same order of magnitude as that of the Mandelstam diagram with the same number of $\phi^3$ vertices.

All the above considerations are also valid for the Reggeon-Reggeon case with 4 particles exchanged in the $t$ channel.

Let us now go into some of the more technical details. The contributions from both diagram 1(b) and diagram 2(a) are of the order $g^{10}s^{-2}(\ln s)^3$ as $s \to \infty$ with fixed $t$. Similarly, the contributions from diagrams 1(c), 2(b), 2(c), and 2(d) are each of the order of $g^{12}s^{-2}(\ln s)^4$. However, all these contributions are cancelled by the corresponding crossed diagrams obtained by exchanging $s$ and $u$; this happens for both the Mandelstam diagrams and the non-Mandelstam diagrams. Thus the resulting contributions are of the orders of $g^{10}s^{-2}(\ln s)^2$ and $g^{12}s^{-2}(\ln s)^3$, respectively. If only the Mandelstam diagrams are kept, the resulting series of leading terms is essentially a geometric series and the summation can be carried out easily. When the additional diagrams are also retained, the series is much more complicated. In fact, the summation of this series cannot be carried out explicitly, and the structure in the complex angular momentum plane must be studied through a non-Fredholm integral equation. For forward scattering $t=0$, there is, in addition to a branch cut, also at least one pole to the right of the branch cut. When $-t$ increases, the pole moves closer to the branch cut, and at some finite value of $|t|$ this pole disappears into the branch cut. The discontinuity across the branch cut is of course quite different from the contributions from the Mandelstam diagrams alone. In view of the presence of the pole, we find the term "Reggeon-particle cut" somewhat misleading; the diagrams are in fact characterized by the presence of the three-particle intermediate states. The properties of such diagrams are discussed in Sec. II.

In Sec. III, we deal with the corresponding diagrams with four-particle intermediate states. These diagrams include in particular the usual double Mandelstam diagrams that give the Reggeon-Reggeon cut. The physics is essentially the same but the details are more complicated. In particular, the signature factors play a role of paramount importance. This fact makes the analysis much more delicate. For this reason, we present in great detail the necessary calculations. In order not to lose sight of the chain of reasoning, which is really quite elementary, we relegate such details to a series of appendixes.

It is perhaps illuminating to rephrase the results of this $\phi^3$ calculation in terms of the Reggeon calculus of Gribov and collaborators.[6, 9, 11] This calculus embodies not only the concept of the Regge cut but also deals with the possibility of repeated Reggeon-particle (and Reggeon-Reggeon) scattering. Such processes can occur in perturbation theory only through non-Mandelstam diagrams. In the language of Reggeon calculus, the study of this paper demonstrates, in the perturbation theory of Feynman diagrams, that such repeated interactions of Reggeons are not small compared to the single Reggeon-particle (or Reggeon-Reggeon) term. In other words, in the sense of leading terms, Reggeon calculus replaces an infinite set of Feynman diagrams with simple vertices by an infinite set of Reggeon diagrams with nonlocal, $s$-independent vertices, which are *not small even in the weak coupling limit*. In order for the so-called hybrid diagrams of Reggeon calculus to be useful, this infinite set must be treated nonperturbatively. This is discussed in Sec. IV.

## II. THREE-PARTICLE INTERMEDIATE STATES

In this section we consider all Feynman diagrams which contribute to the Reggeon-particle cut in leading order. Let $P_1$ and $P_2$ be the momentum of the incoming particles and $P_1'$ and $P_2'$ be the momentum of the outgoing particles; then

$$P_1 + P_2 = P_1' + P_2' \ . \tag{2.1}$$

Define the usual Mandelstam variables

$$s = (P_1 + P_2)^2 \ , \tag{2.2a}$$

$$t = (P_1 - P_1')^2 \ , \tag{2.2b}$$

and

$$u = (P_1 - P_2')^2 \tag{2.2c}$$

[with the metric $(+---)$]. We are interested in the limit $s \to \infty$ with $t$ fixed and nonpositive. Since $t$ is spacelike we may write

$$P_1 - P_1' = (0, 0, \vec{\Delta}) \ , \tag{2.3}$$

where $\vec{\Delta}$ is a two-dimensional vector.

The plan of this section is as follows: In Sec. II A we will recall a few well-known properties of Mandelstam diagrams. Next, in Sec. II B we discuss the tenth-order diagram of Fig. 2(a). We then, in Sec. II C, discuss the role of signature and, in Sec. II D, consider the twelfth-order diagrams of Figs. 2(b), 2(c), and 2(d). In Sec. II E we describe the general class of diagrams which contributes to the Reggeon-particle cut and in Sec. II F we derive an integral equation which sums the contributing diagrams. Finally, in Sec. II G

we demonstrate the existence of the three-particle Regge pole.

### A. Mandelstam diagrams

The leading term in the $s \to \infty$ expansion of the amplitude for the Mandelstam diagram in $2(n+1)$-order perturbation theory ($n \geq 3$) is well known[1,2] to be

$$\mathfrak{M}_M^{(2n+2)} = -2\pi i s^{-2} g^4 \frac{1}{(n-1)!} \ln^{n-1} s \, f_M^{(n)}(\vec{\Delta}) + O(s^{-2}\ln^{n-2} s) , \tag{2.4}$$

where

$$f_M^{(n)}(\vec{\Delta}) = \int \frac{d^2\vec{k}}{2(2\pi)^3} \frac{1}{\vec{k}^2 + m^2} \alpha^{n-1}(\vec{\Delta} - \vec{k}) \tag{2.5}$$

and

$$\alpha(\vec{\Delta}) = g^2 \int \frac{d^2\vec{k}}{2(2\pi)^3} \frac{1}{\vec{k}^2 + m^2} \frac{1}{(\vec{\Delta} - \vec{k})^2 + m^2} . \tag{2.6}$$

The function $f_M^{(n)}(\vec{\Delta})$ may be symbolically represented by the diagram in transverse-momentum space of Fig. 3(a).

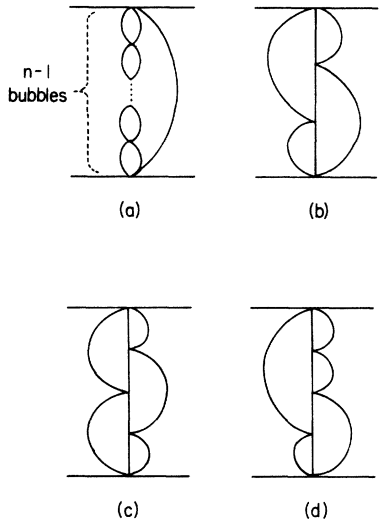


FIG. 3. The transverse diagrams for (a) the $2(n+1)$th-order Mandelstam diagram, (b) the tenth-order diagram 1 of Fig. 2(a), (c) the twelfth-order diagrams 1 and 2 of Figs. 2(b) and 2(c), and (d) the twelfth-order diagram 3 of Fig. 2(d).

### B. Tenth-order non-Mandelstam diagram

The lowest order in which there are important diagrams other than Mandelstam's is tenth, where we have the diagrams of Fig. 2(a). This diagram is analyzed in Appendix B and we find

$$\mathfrak{M}_1^{(10)} = -s^{-2} g^{10} 2\pi i \frac{1}{3!} \ln^3 s \, \tilde{f}_1^{(10)}(\vec{\Delta}) + O(s^{-2}\ln^2 s) , \tag{2.7}$$

where

$$\tilde{f}_1^{(10)}(\vec{\Delta}) = \int \frac{d^2\vec{k}_1}{2(2\pi)^3} \frac{d^2\vec{k}_2}{2(2\pi)^3} \frac{d^2\vec{k}_3}{2(2\pi)^3} \frac{d^2\vec{k}_4}{2(2\pi)^3} (\vec{k}_1^{\,2} + m^2)^{-1} (\vec{k}_2^{\,2} + m^2)^{-1} (\vec{k}_3^{\,2} + m^2)^{-1} (\vec{k}_4^{\,2} + m^2)^{-1} \times [(\vec{\Delta} - \vec{k}_1 - \vec{k}_2)^2 + m^2]^{-1} [(\vec{\Delta} - \vec{k}_2 - \vec{k}_3)^2 + m^2]^{-1} [(\vec{\Delta} - \vec{k}_3 - \vec{k}_4)^2 + m^2]^{-1} . \tag{2.8}$$

This amplitude is represented by the transverse diagram of Fig. 3(b). The amplitude (2.7) is indeed of the same order of magnitude as the Mandelstam amplitude (2.4) with $n = 4$.

### C. Signature

Of course, even in eighth order the Mandelstam diagram of Fig. 1(a) is not the only diagram which contributes, as it is always possible to interchange the $s$ and $u$ channels to obtain the "crossed" diagram of Fig. 4(a). Similarly, for the tenth-order diagram of Sec. II B we have the crossed diagram of Fig. 4(b). For both of these crossed diagrams it is easily verified that the leading term of the $s \to \infty$ expansion is precisely the negative of the leading term (2.4) and (2.7) of the uncrossed diagrams. Therefore, this leading-order expansion for the individual diagrams is not accurate enough to study the sum of all the contributing diagrams.

However, it is not difficult to refine the asymptotic expansion to compute the leading term of the sum of the diagram and the crossed diagram. As shown in Appendix B the expansion (2.7) of $\mathfrak{M}_1^{(10)}$ is more precisely given as

$$\mathfrak{M}_1^{(10)} = -s^{-2} g^{10} 2\pi i \frac{1}{3!} (\ln s - \pi i)^3 \tilde{f}_1^{(10)}(\vec{\Delta}) + A s^{-2}\ln^2 s + O(s^{-2}\ln s) , \tag{2.7'}$$

where $A$ is purely imaginary. Moreover, the expansion of the amplitude for the crossed diagram $\mathfrak{M}_{1c}^{(10)}$ is

$$\mathfrak{M}_{1c}^{(10)} = s^{-2} g^{10} 2\pi i \frac{1}{3!} \ln^3 s \, \tilde{f}_1^{(10)}(\vec{\Delta}) - A s^{-2} \ln^2 s + O(s^{-2} \ln s) \, . \tag{2.9}$$

Therefore $A$ cancels out when we sum $\mathfrak{M}_1^{(10)}$ and $\mathfrak{M}_{1c}^{(10)}$ and we obtain

$$\mathfrak{M}_1^{(10)} + \mathfrak{M}_{1c}^{(10)} = -2\pi^2 s^{-2} g^{10} \tfrac{1}{2} \ln^2 s \, \tilde{f}_1^{(10)}(\vec{\Delta}) + O(s^{-2} \ln s) \, . \tag{2.10}$$

Similarly for the $2(n+2)$-order Mandelstam diagram we have

$$\mathfrak{M}_M^{(2n+4)} + \mathfrak{M}_{Mc}^{(2n+4)} = -2\pi^2 s^{-2} g^4 \frac{1}{(n-1)!} \ln^{n-1} s \, \tilde{f}_M^{(n+1)}(\vec{\Delta}) + O(s^{-2} \ln^{n-2} s) \, . \tag{2.11}$$

### D. Twelfth-order non-Mandelstam diagrams

In twelfth order we consider the three diagrams[22] of Figs. 2(b), 2(c), 2(d) and the three crossed diagrams of Figs. 4(c), 4(d), 4(e). These diagrams are explicitly expanded in Appendixes C, D, and E and we find

$$\mathfrak{M}_1^{(12)} + \mathfrak{M}_{1c}^{(12)} = -2\pi^2 s^{-2} g^{12} \frac{1}{3!} \ln^3 s \, \tilde{f}_1^{(12)}(\vec{\Delta}) + O(s^{-2} \ln^2 s) \, , \tag{2.12}$$

$$\mathfrak{M}_2^{(12)} + \mathfrak{M}_{2c}^{(12)} = \mathfrak{M}_1^{(12)} + \mathfrak{M}_{1c}^{(12)} + O(s^{-2} \ln^2 s) \, , \tag{2.13}$$

and

$$\mathfrak{M}_3^{(12)} + \mathfrak{M}_{3c}^{(12)} = -2\pi^2 s^{-2} g^{12} \frac{1}{3!} \ln^3 s \, \tilde{f}_2^{(12)}(\vec{\Delta}) + O(s^{-2} \ln^2 s) \, , \tag{2.14}$$

where

$$\tilde{f}_1^{(12)}(\vec{\Delta}) = \int \frac{d^2\vec{k}_1}{2(2\pi)^3} \frac{d^2\vec{k}_2}{2(2\pi)^3} \frac{d^2\vec{k}_3}{2(2\pi)^3} \frac{d^2\vec{k}_4}{2(2\pi)^3} \frac{d^2\vec{k}_5}{2(2\pi)^3} (\vec{k}_1^{\,2} + m^2)^{-1} (\vec{k}_2^{\,2} + m^2)^{-1} (\vec{k}_3^{\,2} + m^2)^{-1} (\vec{k}_4^{\,2} + m^2)^{-1} (\vec{k}_5^{\,2} + m^2)^{-1}$$
$$\times [(\vec{\Delta} - \vec{k}_1 - \vec{k}_2)^2 + m^2]^{-1} [(\vec{\Delta} - \vec{k}_2 - \vec{k}_3)^2 + m^2]^{-1} [(\vec{\Delta} - \vec{k}_3 - \vec{k}_4)^2 + m^2]^{-1} [(\vec{\Delta} - \vec{k}_4 - \vec{k}_5)^2 + m^2]^{-1} \tag{2.15}$$

and

$$\tilde{f}_2^{(12)}(\vec{\Delta}) = \int \frac{d^2\vec{k}_1}{2(2\pi)^3} \frac{d^2\vec{k}_2}{2(2\pi)^3} \frac{d^2\vec{k}_3}{2(2\pi)^3} \left\{ \int \frac{d^2\vec{k}}{2(2\pi)^3} (\vec{k}^2 + m^2)^{-1} [(\vec{\Delta} - \vec{k}_1 - \vec{k})^2 + m^2]^{-1} \right\}^2$$
$$\times (\vec{k}_1^{\,2} + m^2)^{-1} (\vec{k}_2^{\,2} + m^2)^{-1} (\vec{k}_3^{\,2} + m^2)^{-1} [(\vec{\Delta} - \vec{k}_1 - \vec{k}_2)^2 + m^2]^{-1} [(\vec{\Delta} - \vec{k}_2 - \vec{k}_3)^2 + m^2]^{-1} \, . \tag{2.16}$$

The transverse diagrams for $\tilde{f}_1^{(12)}$ and $\tilde{f}_2^{(12)}$ are given in Figs. 3(c) and 3(d). Again, these expansions are of the same magnitude as the corresponding expansion (2.11) for the twelfth-order Mandelstam diagram.

### E. The class of contributing diagrams

We now wish to generalize the results of the tenth- and twelfth-order perturbation-theory calculations to arbitrary order. The result is that there is a class of diagrams (which includes the Mandelstam diagrams) that contributes to the leading order.[23] Several examples are given in Fig. 5. The class is described as follows:

(1) From the upper horizontal line draw three vertical lines (labeled "1", "2", and "3" in Fig. 5).

(2) Line 1 (the left-most vertical line) and line 3 (the right-most vertical line) are then immediately connected by a horizontal line.

(3) An arbitrary number of horizontal lines may then be drawn in an arbitrary order between 1 and 2, 1 and 3, and 2 and 3.

(4) The three vertical lines must be connected to the lower horizontal line so that the right- and the left-most vertical lines are connected by a horizontal line. This step can always be carried out in two ways and the two diagrams so constructed transform into each other under $s \rightleftharpoons u$ exchange.

It is clear that the Mandelstam diagrams are the subclass of diagrams obtained by only allowing horizontal lines between particles 1 and 3. It is also clear that the tenth- and twelfth-order non-Mandelstam diagrams of Fig. 2 are included in this class of diagrams.

The contribution of one of these diagrams plus its $s \rightleftharpoons u$ crossed diagram in $2(n+1)$-order perturbation theory is

$$-2\pi^2 s^{-2} g^{2n+2} \frac{1}{(n-2)!} \ln^{n-2} s \times (\text{integral from the transverse diagram}), \tag{2.17}$$

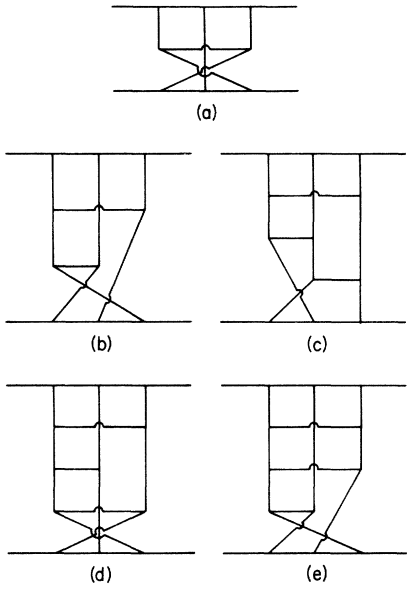


FIG. 4. The $s \leftrightarrow u$ crossed diagrams corresponding to (a) the eighth-order Mandelstam diagram of Fig. 1(a), (b) the tenth-order diagram 1 of Fig. 2(a), (c) the twelfth-order diagram 1 of Fig. 2(b), (d) the twelfth-order diagram 2 of Fig. 2(c), and (e) the twelfth-order diagram 3 of Fig. 2(d).

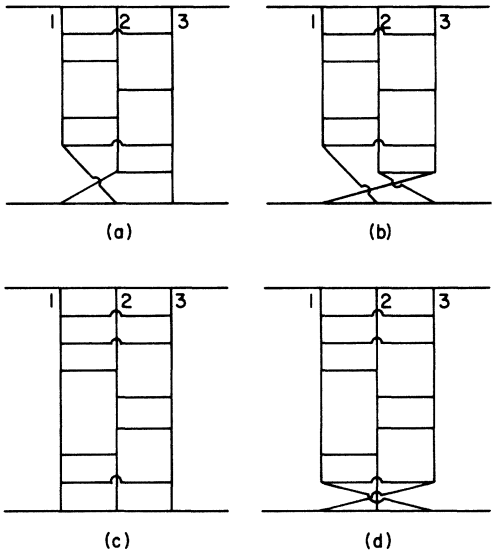


FIG. 5. Four examples of the class of diagrams that are as large as the Mandelstam diagrams when $s \to \infty$: (a) an eighteenth-order diagram, (b) the eighteenth-order diagram obtained from (a) by $s \leftrightarrow u$ exchange, (c) a twentieth-order diagram, and (d) the twentieth-order diagram obtained from (c) by $s \leftrightarrow u$ exchange.

where the transverse diagram is obtained by shrinking all horizontal lines.

### F. Integral equation

We now study the $s \to \infty$ behavior of the sum of the class of diagrams of Sec. II E. For this purpose it is advantageous to pass from $s$ to the conjugate angular momentum variable $j$ by making the Mellin transform

$$\mathfrak{M}(j) = \int_0^\infty ds\, s^{-j-1} \mathfrak{M}(s) \,. \tag{2.18}$$

If for $\mathfrak{M}(s)$ in (2.18) we use

$$\begin{aligned} &\frac{1}{n!} s^{-2} \ln^n s \quad \text{for } 1 < s \,, \\ &0 \qquad\quad \text{for } 0 < s < 1 \,, \end{aligned} \tag{2.19}$$

we have

$$\frac{1}{n!} \int_1^\infty ds\, s^{-3-j} \ln^n s = (2+j)^{-n-1} \,. \tag{2.20}$$

Therefore, using (2.20) we find that in the vicinity of $j = -2$ the Mellin transform of (2.17) is

$$-2\pi^2 g^{2n+2} (j+2)^{-n+1} \times (\text{integral from the transverse diagram}) \,. \tag{2.21}$$

We may now write an integral equation for $\mathfrak{M}(j)$ valid near $j = -2$.

Consider a general transverse diagram and cut all three lines just before they join the bottom line (Fig. 6). With each line there is associated a transverse propagator. Therefore consider the function obtained by omitting the three propagators cut by the dashed line (and the associated integrations). In $(2n+2)$-order perturbation theory

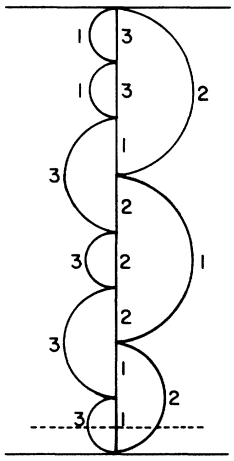


FIG. 6. A typical transverse diagram of twentieth order. The dashed line indicates the cut used to derive the integral equation (2.29).

call this function $f^{(n)}(\vec{k}_1, \vec{k}_2, \vec{k}_3)$, where $\vec{k}_1 + \vec{k}_2 + \vec{k}_3 = \vec{\Delta}$ is the momentum transfer (2.3). From inspection of Fig. 6 we see that, for given $\vec{\Delta}$, $f^{(n)}(\vec{k}_1, \vec{k}_2, \vec{k}_3)$ must of the form

$$f^{(n)}(\vec{k}_1, \vec{k}_2, \vec{k}_3) = f_1^{(n)}(\vec{k}_1) + f_2^{(n)}(\vec{k}_2) + f_3^{(n)}(\vec{k}_3) \ . \quad (2.22)$$

Furthermore, define, for $i = 1, 2, 3$,

$$f_i(k_i) = \sum_{n=3}^{\infty} f_i^{(n)}(\vec{k}_i) \quad (2.23)$$

and

$$f(\vec{k}) = f_1(\vec{k}) + f_2(\vec{k}) + f_3(\vec{k}) \ . \quad (2.24)$$

Then, in terms of the variable

$$\zeta = j + 2 \quad (2.25)$$

the amplitude $\mathfrak{M}(j)$ for the sum of all diagrams of our class is related to $f(\vec{k})$ by

$$\mathfrak{M}(j) = g^2 \zeta^{-1} \int \frac{d^2\vec{k}}{16\pi^3} f(\vec{k}) \frac{1}{\vec{k}^2 + m^2} \alpha(\vec{\Delta} - \vec{k}) \ . \quad (2.26)$$

Furthermore, since our class of diagrams begins with the eighth-order Mandelstam diagram we find from (2.11) that

$$f_1^{(3)}(\vec{k}_1) = f_3^{(3)}(\vec{k}_3) = 0 \quad (2.27a)$$

and

$$f_2^{(3)}(\vec{k}_2) = -2\pi^2 g^2 \zeta^{-1} \alpha(\vec{\Delta} - \vec{k}_2) \ . \quad (2.27b)$$

The functions $f_i^{(n)}(k_i)$ satisfy the recursion relation, for $n \geq 3$,

$$\begin{pmatrix} f_1^{(n+1)}(\vec{k}) \\ f_2^{(n+1)}(\vec{k}) \\ f_3^{(n+1)}(\vec{k}) \end{pmatrix} = \zeta^{-1} \alpha(\vec{\Delta} - \vec{k}) \begin{pmatrix} f_1^{(n)}(\vec{k}) \\ f_2^{(n)}(\vec{k}) \\ f_3^{(n)}(\vec{k}) \end{pmatrix} + \zeta^{-1} g^2 \int \frac{d^2\vec{k}'}{2(2\pi)^3} \frac{1}{\vec{k}'^2 + m^2} \frac{1}{(\vec{\Delta} - \vec{k} - \vec{k}')^2 + m^2} \begin{pmatrix} 0 & 1 & 1 \\ 1 & 0 & 1 \\ 1 & 1 & 0 \end{pmatrix} \begin{pmatrix} f_1^{(n)}(\vec{k}') \\ f_2^{(n)}(\vec{k}') \\ f_3^{(n)}(\vec{k}') \end{pmatrix} \ . \quad (2.28)$$

Therefore, summing over $n$ and using the initial condition (2.27) we obtain the desired equation for $f_i(\vec{k})$

$$[1 - \zeta^{-1}\alpha(\vec{\Delta} - \vec{k})] \begin{pmatrix} f_1(\vec{k}) \\ f_2(\vec{k}) \\ f_3(\vec{k}) \end{pmatrix} = \begin{pmatrix} 0 \\ -2\pi^2 g^2 \zeta^{-1} \alpha(\vec{\Delta} - \vec{k}) \\ 0 \end{pmatrix} + \zeta^{-1} g^2 \int \frac{d^2\vec{k}'}{2(2\pi)^3} \frac{1}{\vec{k}'^2 + m^2} \frac{1}{(\vec{\Delta} - \vec{k} - \vec{k}')^2 + m^2} \begin{pmatrix} 0 & 1 & 1 \\ 1 & 0 & 1 \\ 1 & 1 & 0 \end{pmatrix} \begin{pmatrix} f_1(\vec{k}') \\ f_2(\vec{k}') \\ f_3(\vec{k}') \end{pmatrix} \quad (2.29)$$

from which, by adding together the three equations, we obtain the integral equation for $f(\vec{k})$,

$$[1 - \zeta^{-1}\alpha(\vec{\Delta} - \vec{k})] f(\vec{k}) = -2\pi^2 g^2 \zeta^{-1} \alpha(\vec{\Delta} - \vec{k}) + 2\zeta^{-1} g^2 \int \frac{d^2\vec{k}'}{16\pi^3} \frac{1}{\vec{k}'^2 + m^2} \frac{1}{(\vec{\Delta} - \vec{k} - \vec{k}')^2 + m^2} f(\vec{k}') \ . \quad (2.30)$$

### G. Three-particle Regge pole

We conclude Sec. II by studying the singularities of $\mathfrak{M}(j)$.

Consider first the equation obtained from (2.30) by omitting the last term. This is the equation we would obtain if we considered only the Mandelstam diagram. The equation is easily solved and, calling $\mathfrak{M}_M(j)$ the resulting amplitude, we find

$$\mathfrak{M}_M(j) = -2\pi^2 g^4 \zeta^{-2} \int \frac{d^2\vec{k}}{16\pi^3} \frac{1}{\vec{k}^2 + m^2} \frac{\alpha^2(\vec{\Delta} - \vec{k})}{1 - \zeta^{-1}\alpha(\vec{\Delta} - \vec{k})} , \quad (2.31)$$

which clearly has a branch point at

$$j = -2 + \alpha(0) \ . \quad (2.32)$$

This branch cut is known in the literature as the Reggeon-particle cut.

We now demonstrate that, in fact, the full amplitude $\mathfrak{M}(j)$ has a pole to the right of this cut when $\vec{\Delta}$ is not too large.

The amplitude $\mathfrak{M}(j)$ will have a pole if $f(\vec{k})$ has a pole for some value of $\zeta = \alpha_3(\vec{\Delta})$. At this three-particle Regge pole, the inhomogeneous term in (2.30) is to be neglected and thus the homogeneous equation

$$[1 - \alpha_3^{-1}(\vec{\Delta})\, \bar{\alpha}(\vec{\Delta} - \vec{k})] f_0(\vec{k}) = 2\alpha_3^{-1}(\vec{\Delta}) g^2 \int \frac{d^2\vec{k}'}{16\pi^3} \frac{1}{\vec{k}'^2 + m^2} \frac{1}{(\vec{\Delta} - \vec{k} - \vec{k}')^2 + m^2} f_0(\vec{k}') \quad (2.33)$$

has a nontrivial solution $f_0(\vec{k})$. Define

$$\bar{\alpha}(\vec{\Delta} - \vec{k}) = g^{-2} 16\pi^3 \alpha(\vec{\Delta} - \vec{k}) \quad (2.34)$$

and

$$\lambda = g^{-2} 16\pi^3 \alpha_3(\vec{\Delta}) \ . \quad (2.35)$$

Then multiply (2.33) by $\lambda$ to obtain an equation with no coupling constant,

$$[\lambda - \bar{\alpha}(\vec{\Delta}-\vec{k})]f_0(\vec{k}) = 2\int d^2k' \frac{1}{\vec{k}'^2+m^2} \times \frac{1}{(\vec{\Delta}-\vec{k}-\vec{k}')^2+m^2} f_0(\vec{k}'). \tag{2.36}$$

Symmetrize (2.36) by defining

$$h(\vec{k}) = (\vec{k}^2+m^2)^{-1/2} f_0(\vec{k}) \tag{2.37}$$

so that

$$[\lambda - \bar{\alpha}(\vec{\Delta}-\vec{k})]h(\vec{k}) = 2\int d^2\vec{k}'(\vec{k}^2+m^2)^{-1/2} \times (\vec{k}'^2+m^2)^{-1/2} \times \frac{h(\vec{k}')}{(\vec{\Delta}-\vec{k}-\vec{k}')^2+m^2} . \tag{2.38}$$

This integral equation may be obtained by a variational principle. Therefore we find that the largest eigenvalue $\lambda_{\max}$ obeys

$$\lambda_{\max} = \sup_h \left\{ \left[ \int d^2\vec{k} h^2(\vec{k})\, \alpha(\vec{\Delta}-\vec{k}) + 2\iint d^2\vec{k}\, d^2\vec{k}' (\vec{k}'^2+m^2)^{-1/2}(\vec{k}^2+m^2)^{-1/2} \frac{h(\vec{k})h(\vec{k}')}{(\vec{\Delta}-\vec{k}-\vec{k}')^2+m^2} \right] \left[ \int d^2\vec{k} h^2(\vec{k}) \right]^{-1} \right\} . \tag{2.39}$$

To demonstrate that

$$\lambda_{\max} > \bar{\alpha}(0) = \pi m^{-2} \tag{2.40}$$

it suffices to use as a trial function in (2.39)

$$\tilde{h}(\vec{k}) = \begin{cases} 1 & \text{if } |\vec{k}-\vec{\Delta}| < a , \\ 0 & \text{otherwise} . \end{cases} \tag{2.41}$$

Then we have the estimate

$$\iint d^2\vec{k}\, d^2\vec{k}' (\vec{k}'^2+m^2)^{-1/2}(\vec{k}^2+m^2)^{-1/2} \frac{\tilde{h}(\vec{k})\tilde{h}(\vec{k}')}{(\vec{\Delta}-\vec{k}-\vec{k}')^2+m^2} \geq [(|\vec{\Delta}|+a)^2+m^2]^{-1}[(|\vec{\Delta}|+2a)^2+m^2]^{-1}(\pi a^2)^2 . \tag{2.42}$$

Moreover, if we use the inequality valid for $x > -1$

$$\frac{1}{1+x} \geq 1 - x + x^2 - x^3 \tag{2.43}$$

we find that

$$\int d^2\vec{q}\, \tilde{h}(\vec{q})\, \bar{\alpha}(\vec{\Delta}-\vec{q}) = \int_{|k|<a} d^2\vec{k} \int d^2\vec{k}' \frac{1}{\vec{k}'^2+m^2} \frac{1}{\vec{k}'^2+m^2-2\vec{k}\cdot\vec{k}'+\vec{k}^2} \geq \pi^2 a^2 m^{-2}(1 - \tfrac{1}{12}a^2m^{-2} - \tfrac{1}{18}a'^4m^{-4} - \tfrac{1}{16}a^6m^{-6}) . \tag{2.44}$$

Therefore, using (2.42) and (2.44) in (2.39) we find

$$\lambda_{\max} - \bar{\alpha}(0) > \max_a \pi a^2 \left\{ \frac{2}{[(|\vec{\Delta}|+a)^2+m^2][(|\vec{\Delta}|+2a)^2+m^2]} - \frac{1}{12m^4} - \frac{1}{18}a^2m^{-6} - \frac{1}{16}a^4m^{-8} \right\} . \tag{2.45}$$

The expression on the right-hand side is positive for sufficiently small values of $a$ if

$$\vec{\Delta}^2 m^{-2} < 2\sqrt{6} - 1 . \tag{2.46}$$

Hence it follows that if $\vec{\Delta}$ satisfies (2.46), then the amplitude $\mathfrak{M}(j)$ has a three-particle Regge pole which lies to the right of the Mandelstam cut.

## III. FOUR-PARTICLE INTERMEDIATE STATES

We now turn our attention to the case of four-particle intermediate states in the $t$ channel. Our results are qualitatively the same as those of Sec. II. In particular we show the following:

(1) The class of diagrams which contributes to the leading order as $s \to \infty$ is much larger than the class of double Mandelstam diagrams illustrated in Fig. 7.

(2) When the momentum transfer $\vec{\Delta}$ is zero, the singularity of the amplitude in the $j$ plane which is farthest to the right is not the "Reggeon-Reggeon" cut at

$$j = -3 + 2\alpha(0) , \tag{3.1}$$

because there is a cut due to the convolution of the three-particle Reggeon of Sec. II G with an additional elementary particle which lies to the right of (3.1).

This case of "Reggeon-Reggeon" scattering has been extensively discussed by previous authors.[8] Our treatment differs from these previous treatments in two respects:

(1) Many diagrams previously thought to be negligible are demonstrated to be important.

(2) The effects of signature are properly taken into account. These signature effects are particularly important for the diagrams which previous authors thought were small.

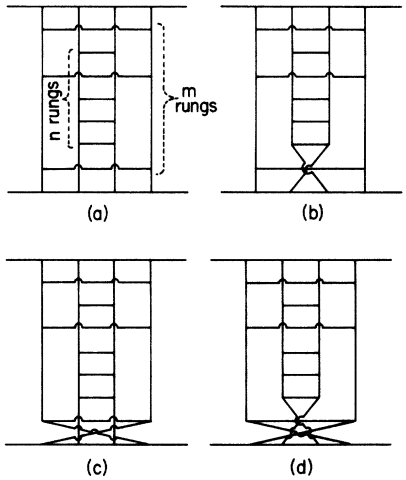


FIG. 7. Double Mandelstam diagrams with $m$ rungs in the outer ladder and $n$ rungs in the inner ladder. Diagrams (c) and (d) are obtained from diagrams (b) and (a), respectively, by $s \longleftrightarrow u$.

### A. Double Mandelstam diagrams

The diagrams analogous to the Mandelstam diagrams for the exchange of a Regge pole and a particle are the double Mandelstam diagrams of Fig. 7. These diagrams have been analyzed by Cicuta and Sugar[24] and by Hasslacher and Sinclair.[25] They find for the general diagram of Fig. 7 with $m$ rungs in the outer ladder and $n$ rungs in the inner ladder that, for $m \geq 1$ and $n \geq 0$,

$$\mathfrak{M}_{M_1}^{2(m+n+4)} = -\eta_{m,n} g^4 2\pi i s^{-3} \ln^{n+m+2} s \left[ \frac{1}{(n+1)!} \frac{1}{(m+1)!} f_{m+1,n+1}(\vec{\Delta}) + 2 \frac{1}{(n+2)!} \frac{1}{m!} f_{m,n+2}(\vec{\Delta}) + \frac{1}{(n+3)!} \frac{1}{(m-1)!} f_{m-1,n+3}(\vec{\Delta}) \right] + O(s^{-3} \ln^{n+m+1} s), \tag{3.2}$$

where for $m \neq 0$

$$f_{m,n}(\vec{\Delta}) = \int \frac{d^2\vec{k}}{16\pi^3} \alpha^m(\vec{k}) \alpha^n(\vec{\Delta} - \vec{k}) , \tag{3.3a}$$

$$f_{0,n}(\vec{\Delta}) = 0 , \tag{3.3b}$$

and

$$\eta_{m,n} = \begin{cases} \frac{1}{2} & \text{if } m = n+2 , \\ 1 & \text{otherwise} . \end{cases} \tag{3.4}$$

We note that the method of specifying diagrams given by Fig. 7 is not unique and that the diagrams specified by $(m, n)$ and by $(n+2, m-2)$ are the same. Therefore, when (3.2) is summed over $m$ and $n$, one must divide by two to avoid double counting.

Along with the diagrams of Fig. 7(a) we must also consider the three additional diagrams obtained by twisting the legs of the ladders as shown in Figs. 7(b), 7(c), and 7(d). These four diagrams are each of the order $g^{2(m+n+4)} s^{-3} \ln^{n+m+2} s$. However, when added together their sum is only of the order $g^{2(m+n+4)} s^{-3} \ln^{m+n} s$. This loss of two powers of ln$s$ is expected on the basis of considerations of the signature of each constituent ladder. Calling the four separate amplitudes of Fig. 7 1, 2, 3 and 4, respectively, we find[24, 25]

$$\sum_{i=1}^{4} \mathfrak{M}_{M_i}^{2(m+n+4)} = -\eta_{m,n} g^4 2(\pi i)^3 s^{-3} \ln^{n+m} s \left[ \frac{1}{n!} \frac{1}{m!} f_{m+1,n+1}(\vec{\Delta}) + 2 \frac{1}{(n+1)!} \frac{1}{(m-1)!} f_{m,n+2}(\vec{\Delta}) + \frac{1}{(n+2)!} \frac{1}{(m-2)!} f_{m-1,n+3}(\vec{\Delta}) \right] + O(s^{-3} \ln^{n+m-1} s) . \tag{3.5}$$

### B. Non-Mandelstam diagrams

The lowest order in which there are non-Mandelstam diagrams which are comparable to the double Mandelstam diagrams of Fig. 7 is twelfth order. These lowest-order diagrams are given in Fig. 8 and are obtained by adding a vertical line to the tenth-order non-Mandelstam diagrams of Fig. 2(a) in all possible ways plus the crossed diagrams. We note that the diagrams of Fig. 8(b) and 8(c) are their own crossed diagrams.

We could go on systematically and calculate these four twelfth-order diagrams. However, since the calculations are somewhat tedious we will proceed directly to a diagram (Fig. 9) of particular interest which has been discussed incorrectly in the literature.[8] This twentieth-order diagram is surely one which should be considered in an attempt to study the interaction of two Reggeons. The calculation of the $s \to \infty$ behavior of this diagram is somewhat subtle. We carry it out in Appendix F and find that it behaves as

$$-ig^{20}s^{-3}\ln^{7}s\, f(\vec{\Delta})\,. \tag{3.6}$$

Moreover, $f(\vec{\Delta})$ does *not* have a natural representation in terms of an amplitude in transverse-momentum space.

By itself the diagram of Fig. 9 is one power of $\ln s$ smaller than the twentieth-order double Mandelstam diagrams [(3.2) with $m+n=6$]. However, (3.6) is one power of $\ln s$ larger than the sum (3.5) of all four double Mandelstam diagrams which must be added together to obtain the correct signature factors. This clearly indicates that in addition to the diagram of Fig. 9 we must consider other diagrams as well.

We obtain further insight into the diagram of Fig. 9 by straightening out the top and bottom lines as shown in Fig. 10. (There are, of course, 3 other possible ways to straighten out these lines and each way must, in general, be discussed separately. See Appendix F.) In this form it is clear that we should consider the signature partner diagram obtained from Fig. 10 by

(a) transposing at the upper end the two interior vertical lines,

(b) transposing at the lower end the two interior vertical lines, or

(c) transposing the two interior lines at both the top and the bottom.

These diagrams are shown in Figs. 11, 12, and 13 (see Appendix G). Furthermore, there are the additional diagrams obtained from these by $s \leftrightarrow u$ crossing.

These diagrams are treated in Appendixes F and G. It is found that each of these non-Mandelstam diagrams is of order $g^{20}s^{-3}\ln^{7}s$. We also find that the diagrams obtained by transposing the upper or the lower interior pair of lines are both purely imaginary in leading order. However, if both the upper and the lower ends are transposed, there is also a real part to the amplitude. When we sum these four amplitudes together the imaginary parts cancel and the result (G10) is of the form

$$g^{20}s^{-3}\ln^{7}s\, \bar{f}(\vec{\Delta})\,, \tag{3.7}$$

where $\bar{f}(\vec{\Delta})$ is real and *is* representable as an amplitude in transverse momentum space (Fig. 14). Now when we add the four $s \leftrightarrow u$ crossed diagrams we lose a power of $\ln s$ and gain a factor of $i$ so the final result is proportional to

$$-ig^{20}s^{-3}\ln^{6}s\, \bar{f}(\vec{\Delta})\,. \tag{3.8}$$

This has exactly the same power of $\ln s$ as does the

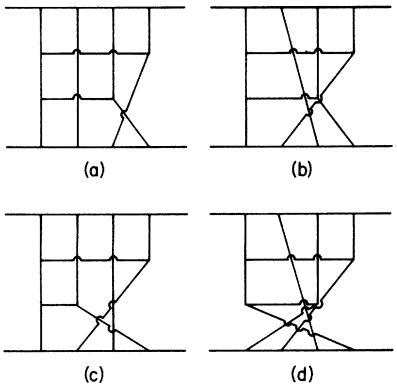


FIG. 8. The four twelfth-order diagrams which are comparable to the twelfth-order double Mandelstam diagrams of Fig. 7.

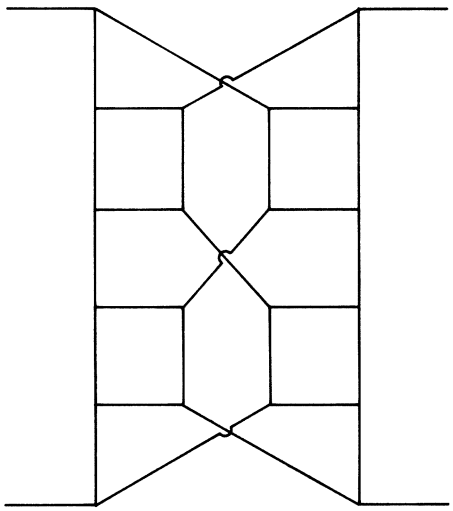

FIG. 9. A twentieth-order diagram that contributes to Reggeon-Reggeon scattering.

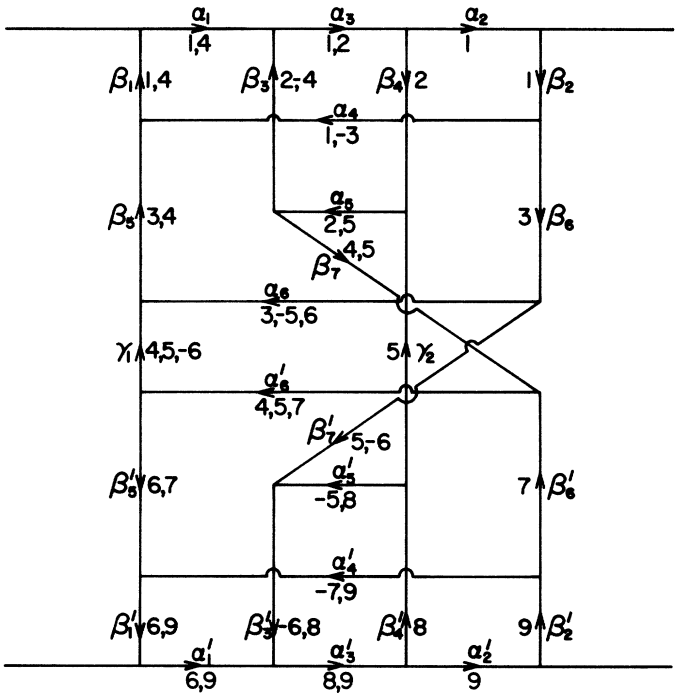


FIG. 10. The diagram of Fig. 9 redrawn in a useful fashion. The Feynman parameters indicated are used in the calculation of Appendix F.

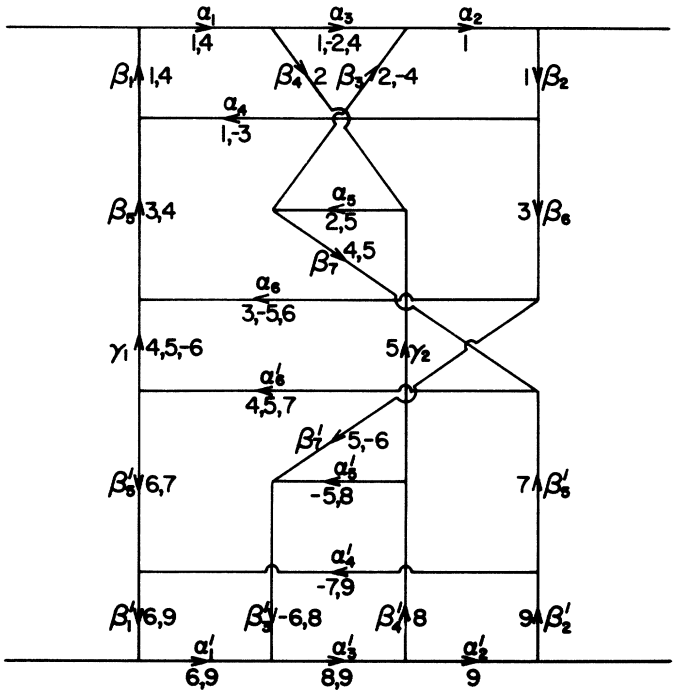


FIG. 11. The diagram obtained from that of Fig. 10 by transposing the two inner vertical lines at the top.

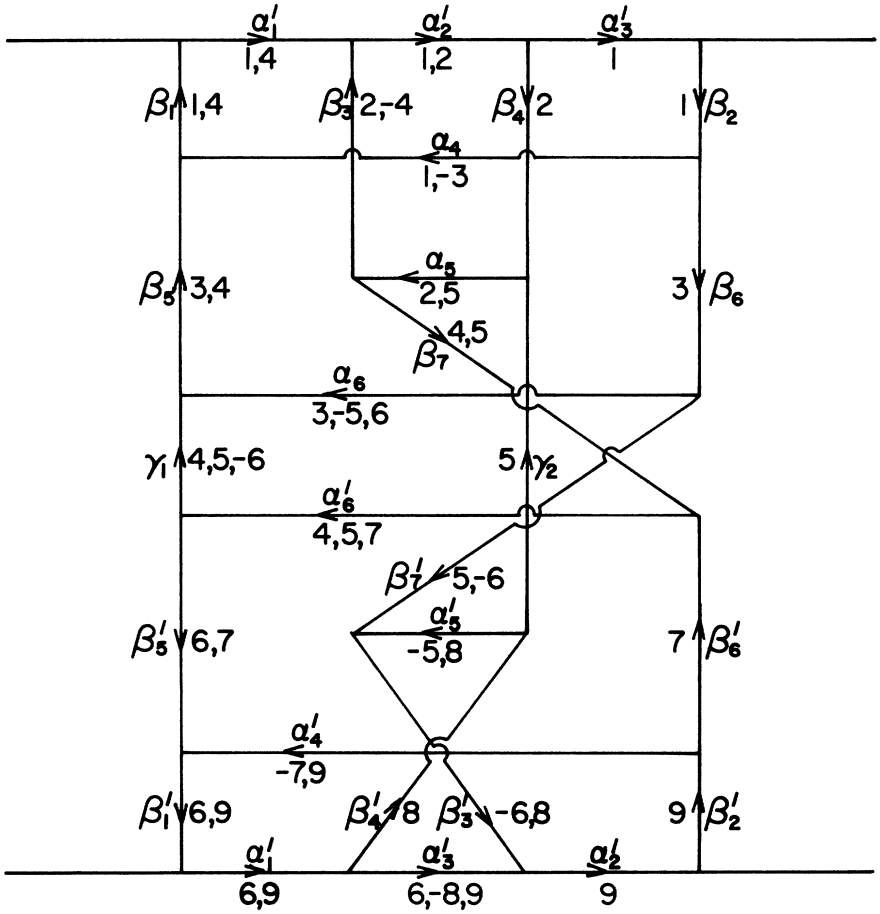


FIG. 12. The diagram obtained from that of Fig. 10 by transposing the two inner vertical lines at the bottom.

sum (3.5) of the double Mandelstam diagrams of twentieth order.

In general, the class of contributing diagrams is described as follows:

(1) Draw 4 vertical lines from the upper horizontal line.

(2) Connect the outer two lines by a horizontal line.

(3) Draw any number of horizontal lines between lines (1, 2), (1, 3), (1, 4), (2, 3), (2, 4), and (3, 4) in any order whatsoever.

(4) Join the 4 vertical lines to the bottom horizontal line in such a fashion that the outer two lines are connected by a horizontal line.

As in the previous example, when we add together the amplitudes of the diagram and its signature partners we obtain a result which is proportional to the amplitude of the transverse diagram obtained by contracting all horizontal lines.

The sign of all contributions is the same. This is a reflection of the fact that $\phi^3$ is a theory of *attractive* bosons.

### C. Integral equation

The sum of all these contributions is given by an integral equation analogous to that of Sec. II F. In particular, consider the amplitude obtained by cutting a transverse diagram at the bottom. Calling this amplitude $f(\vec{k}_1, \vec{k}_2, \vec{k}_3, \vec{k}_4)$, with

$$\vec{k}_1 + \vec{k}_2 + \vec{k}_3 + \vec{k}_4 = \vec{\Delta} , \tag{3.9}$$

we have, for given $\vec{\Delta}$,

$$f(\vec{k}_1, \vec{k}_2, \vec{k}_3, \vec{k}_4) = f_{12}(\vec{k}_1, \vec{k}_2) + f_{13}(\vec{k}_1, \vec{k}_3) + f_{14}(\vec{k}_1, \vec{k}_4) + f_{23}(\vec{k}_2, \vec{k}_3) + f_{24}(\vec{k}_2, \vec{k}_4) + f_{34}(\vec{k}_3, \vec{k}_4) , \tag{3.10}$$

where

$$f_{ll'}(\vec{k}_l, \vec{k}_{l'}) = f_{ll'}(\vec{k}_{l'}, \vec{k}_l) . \tag{3.11}$$

Then for the Mellin transform $\mathfrak{M}(j)$ we have, with

$$\zeta = j + 3 , \tag{3.12}$$

$$\mathfrak{M}(j) = \sum_{1\le l<l'\le 4} g^4\zeta^{-1}\int \frac{d^3\vec{k}_l}{16\pi^3}\,\frac{d^2\vec{k}_{l'}}{16\pi^3}\, f_{l',l}(\vec{k}_{l'},\vec{k}_l)\,\frac{1}{\vec{k}_l^{\,2}+m^2}\,\frac{1}{\vec{k}_{l'}^{\,2}+m^2}\,\alpha(\vec{\Delta}-\vec{k}_l-\vec{k}_{l'})$$

$$= g^4\zeta^{-1}\int \frac{d^2\vec{k}}{16\pi^3}\,\frac{d^2\vec{k}'}{16\pi^3}\, f(\vec{k},\vec{k}')\,\frac{1}{\vec{k}^2+m^2}\,\frac{1}{\vec{k}'^2+m^2}\,\alpha(\vec{\Delta}-\vec{k}-\vec{k}')\,, \tag{3.13}$$

where

$$f(\vec{k},\vec{k}') = \sum_{1\le l<l'\le 4} f_{l'l}(\vec{k},\vec{k}')\,. \tag{3.14}$$

Furthermore, calling $f_{ll'}^{(n)}(\vec{k}_l,\vec{k}_{l'})$ the amplitude in $2(n+4)$-order perturbation theory, we find

$$f_{12}^{(1)} = f_{13}^{(1)} = f_{14}^{(1)} = f_{24}^{(1)} = f_{34}^{(1)} = 0 \tag{3.15a}$$

and

$$f_{23}^{(1)}(\vec{k}_2,\vec{k}_3) = -2\pi^3 i\zeta^{-1}g^2\alpha(\vec{\Delta}-\vec{k}_2-\vec{k}_3)\,. \tag{3.15b}$$

Then the $f_{l,l}^{(n)}$ satisfy the recursion relation

$$\begin{pmatrix} f_{12}^{(n+1)}(\vec{k},\vec{k}') \\ f_{13}^{(n+1)}(\vec{k},\vec{k}') \\ f_{14}^{(n+1)}(\vec{k},\vec{k}') \\ f_{23}^{(n+1)}(\vec{k},\vec{k}') \\ f_{24}^{(n+1)}(\vec{k},\vec{k}') \\ f_{34}^{(n+1)}(\vec{k},\vec{k}') \end{pmatrix} = \zeta^{-1}\alpha(\vec{\Delta}-\vec{k}-\vec{k}') \begin{pmatrix} f_{12}^{(n)}(\vec{k},\vec{k}') \\ f_{13}^{(n)}(\vec{k},\vec{k}') \\ f_{14}^{(n)}(\vec{k},\vec{k}') \\ f_{23}^{(n)}(\vec{k},\vec{k}') \\ f_{24}^{(n)}(\vec{k},\vec{k}') \\ f_{34}^{(n)}(\vec{k},\vec{k}') \end{pmatrix}$$

$$+\zeta^{-1}g^2\int \frac{d^2\vec{k}''}{16\pi^3}\,\frac{1}{\vec{k}''^2+m^2}\,\frac{1}{(\vec{\Delta}-\vec{k}-\vec{k}'-\vec{k}'')^2+m^2} \begin{pmatrix} 0&0&0&0&0&1\\ 0&0&0&0&1&0\\ 0&0&0&1&0&0\\ 0&0&1&0&0&0\\ 0&1&0&0&0&0\\ 1&0&0&0&0&0 \end{pmatrix} \begin{pmatrix} f_{12}^{(n)}(\vec{k}'',\vec{\Delta}-\vec{k}-\vec{k}'-\vec{k}'') \\ f_{13}^{(n)}(\vec{k}'',\vec{\Delta}-\vec{k}-\vec{k}'-\vec{k}'') \\ f_{14}^{(n)}(\vec{k}'',\vec{\Delta}-\vec{k}-\vec{k}'-\vec{k}'') \\ f_{23}^{(n)}(\vec{k}'',\vec{\Delta}-\vec{k}-\vec{k}'-\vec{k}'') \\ f_{24}^{(n)}(\vec{k}'',\vec{\Delta}-\vec{k}-\vec{k}'-\vec{k}'') \\ f_{34}^{(n)}(\vec{k}'',\vec{\Delta}-\vec{k}-\vec{k}'-\vec{k}'') \end{pmatrix}$$

$$+\zeta^{-1}g^2\int \frac{d^2\vec{k}''}{16\pi^3}\,\frac{1}{\vec{k}''^2+m^2}\,\frac{1}{(\vec{\Delta}-\vec{k}-\vec{k}'-\vec{k}'')^2+m^2}\,\frac{1}{2} \begin{pmatrix} 0&1&1&1&1&0\\ 1&0&1&1&0&1\\ 1&1&0&0&1&1\\ 1&1&0&0&1&1\\ 1&0&1&1&0&1\\ 0&1&1&1&1&0 \end{pmatrix} \begin{pmatrix} f_{12}^{(n)}(\vec{k},\vec{k}'')+f_{12}^{(n)}(\vec{k}',\vec{k}'') \\ f_{13}^{(n)}(\vec{k},\vec{k}'')+f_{13}^{(n)}(\vec{k}',\vec{k}'') \\ f_{14}^{(n)}(\vec{k},\vec{k}'')+f_{14}^{(n)}(\vec{k}',\vec{k}'') \\ f_{23}^{(n)}(\vec{k},\vec{k}'')+f_{23}^{(n)}(\vec{k}',\vec{k}'') \\ f_{24}^{(n)}(\vec{k},\vec{k}'')+f_{24}^{(n)}(\vec{k}',\vec{k}'') \\ f_{34}^{(n)}(\vec{k},\vec{k}'')+f_{34}^{(n)}(\vec{k}',\vec{k}'') \end{pmatrix}\,. \tag{3.16}$$

Summing (3.16) on $n$ from 1 to $\infty$ and using the initial condition (3.15) we obtain

$$\begin{bmatrix} f_{12}(\vec{k},\vec{k}') \\ f_{13}(\vec{k},\vec{k}') \\ f_{14}(\vec{k},\vec{k}') \\ f_{23}(\vec{k},\vec{k}') \\ f_{24}(\vec{k},\vec{k}') \\ f_{34}(\vec{k},\vec{k}') \end{bmatrix} [1-\zeta^{-1}\alpha(\vec{\Delta}-\vec{k}-\vec{k}')]$$

$$= \begin{bmatrix} 0 \\ 0 \\ 0 \\ -2\pi^3 i\zeta^{-1}g^2\alpha(\vec{\Delta}-\vec{k}-\vec{k}') \\ 0 \\ 0 \end{bmatrix}$$

$$+\zeta^{-1}g^2\int\frac{d^2\vec{k}''}{16\pi^3}\,\frac{1}{\vec{k}''^2+m^2}\,\frac{1}{(\vec{\Delta}-\vec{k}-\vec{k}'-\vec{k}'')^2+m^2} \begin{bmatrix} 0&0&0&0&0&1 \\ 0&0&0&0&1&0 \\ 0&0&0&1&0&0 \\ 0&0&1&0&0&0 \\ 0&1&0&0&0&0 \\ 1&0&0&0&0&0 \end{bmatrix} \begin{bmatrix} f_{12}(\vec{k}'',\vec{\Delta}-\vec{k}-\vec{k}'-\vec{k}'') \\ f_{13}(\vec{k}'',\vec{\Delta}-\vec{k}-\vec{k}'-\vec{k}'') \\ f_{14}(\vec{k}'',\vec{\Delta}-\vec{k}-\vec{k}'-\vec{k}'') \\ f_{23}(\vec{k}'',\vec{\Delta}-\vec{k}-\vec{k}'-\vec{k}'') \\ f_{24}(\vec{k}'',\vec{\Delta}-\vec{k}-\vec{k}'-\vec{k}'') \\ f_{34}(\vec{k}'',\vec{\Delta}-\vec{k}-\vec{k}'-\vec{k}'') \end{bmatrix}$$

$$+\zeta^{-1}g^2\int\frac{d^2\vec{k}''}{16\pi^3}\,\frac{1}{\vec{k}''^2+m^2}\,\frac{1}{(\vec{\Delta}-\vec{k}-\vec{k}'-\vec{k}'')^2+m^2}\,\frac{1}{2} \begin{bmatrix} 0&1&1&1&1&0 \\ 1&0&1&1&0&1 \\ 1&1&0&0&1&1 \\ 1&1&0&0&1&1 \\ 1&0&1&1&0&1 \\ 0&1&1&1&1&0 \end{bmatrix} \begin{bmatrix} f_{12}(\vec{k},\vec{k}'')+f_{12}(\vec{k}',\vec{k}'') \\ f_{13}(\vec{k},\vec{k}'')+f_{13}(\vec{k}',\vec{k}'') \\ f_{14}(\vec{k},\vec{k}'')+f_{14}(\vec{k}',\vec{k}'') \\ f_{23}(\vec{k},\vec{k}'')+f_{23}(\vec{k}',\vec{k}'') \\ f_{24}(\vec{k},\vec{k}'')+f_{24}(\vec{k}',\vec{k}'') \\ f_{34}(\vec{k},\vec{k}'')+f_{34}(\vec{k}',\vec{k}'') \end{bmatrix}. \quad (3.17)$$

We may now add together all six of these equations and obtain the desired equation for $f(\vec{k},\vec{k}')$ of (3.14)

$$f(\vec{k},\vec{k}')[1-\zeta^{-1}\alpha(\vec{\Delta}-\vec{k}-\vec{k}')] = -2\pi^3 i\zeta^{-1}g^2\alpha(\vec{\Delta}-\vec{k}-\vec{k}')$$
$$+\zeta^{-1}g^2\int\frac{d^2\vec{k}''}{16\pi^3}\,\frac{1}{\vec{k}''^2+m^2}\,\frac{1}{(\vec{\Delta}-\vec{k}-\vec{k}'-\vec{k}'')^2+m^2}\{f(\vec{k}'',\vec{\Delta}-\vec{k}-\vec{k}'-\vec{k}'')$$
$$+2[f(\vec{k}',\vec{k}'')+f(\vec{k},\vec{k}'')]\}\,. \quad (3.18)$$

It is instructive to consider what this equation becomes if we consider summing only the Mandelstam graphs. Then the term containing $f(\vec{k},\vec{k}'')+f(\vec{k}',\vec{k}'')$ is omitted, and calling the resulting function $f_M(\vec{k},\vec{k}')$ we see that $f_M(\vec{k},\vec{k}')$ obeys an equation that depends on $\vec{k}$ and $\vec{k}'$ only through

$$\vec{k}+\vec{k}'=\vec{q}\,. \quad (3.19)$$

Therefore, calling

$$\bar{f}_M(\vec{q})=f_M(\vec{k},\vec{k}') \quad (3.20)$$

we find from (3.18) that

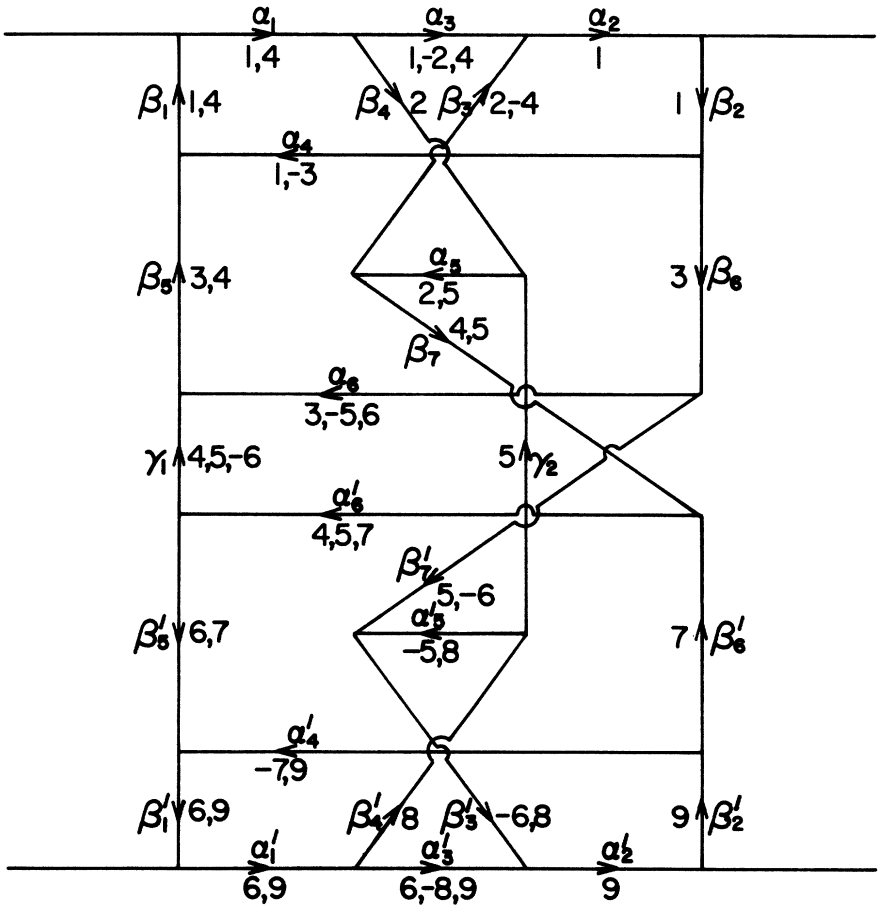


FIG. 13. The diagram obtained from that of Fig. 10 by transposing the inner vertical lines both at the top and at the bottom.

$$\bar{f}_M(\vec{q})[1-\zeta^{-1}\alpha(\vec{\Delta}-\vec{q})] = -2\pi^3 i\zeta^{-1}g^2\alpha(\vec{\Delta}-\vec{q}) + \bar{f}_M(\vec{\Delta}-\vec{q})\,\zeta^{-1}\alpha(\vec{\Delta}-\vec{q}) \tag{3.21}$$

To solve this write the companion equation with $\vec{q} \to \vec{\Delta}-\vec{q}$,

$$\bar{f}_M(\vec{\Delta}-\vec{q})[1-\zeta^{-1}\alpha(\vec{q})] = -2\pi^3 i\zeta^{-1}g^2\alpha(\vec{q}) + \bar{f}_M(\vec{q})\zeta^{-1}\alpha(\vec{q})\ . \tag{3.22}$$

Eliminating $\bar{f}_M(\vec{\Delta}-\vec{q})$ between these equations, we get

$$\bar{f}_M(\vec{q}) = \frac{-2\pi^3 i\zeta^{-1}g^2\alpha(\vec{\Delta}-\vec{q})}{1-\zeta^{-1}[\alpha(\vec{\Delta}-\vec{q})+\alpha(\vec{q})]}\ . \tag{3.23}$$

Therefore using this in (3.13) we obtain the known result for the sum of the double Mandelstam diagrams

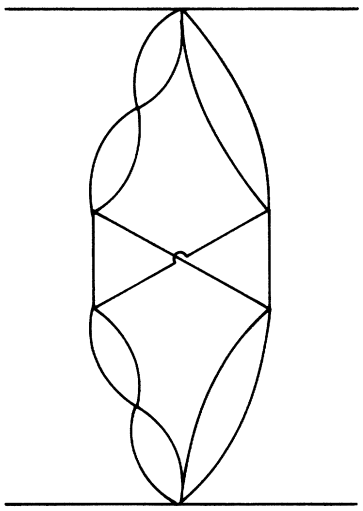

FIG. 14. The transverse diagram for the function $\bar{f}(\vec{\Delta})$.

$$\mathfrak{M}(j) = -g^4\zeta^{-2}2\pi^3 i \int \frac{d^2\vec{q}}{16\pi^3} \frac{\alpha^2(\vec{\Delta}-\vec{q})\alpha(\vec{q})}{1-\zeta^{-1}[\alpha(\vec{\Delta}-\vec{q})+\alpha(\vec{q})]} . \tag{3.24}$$

We conclude by discussing the singularities of $\mathfrak{M}(j)$. When $\vec{\Delta}=0$ we see from (3.24) that $\mathfrak{M}_M(j)$ has a branch point at

$$\zeta = 2\alpha(0) . \tag{3.25}$$

This branch point is expected to remain in the full amplitude $\mathfrak{M}(j)$. However, included in $\mathfrak{M}(j)$ are all diagrams which convolve a single elementary particle with the sum of all three-line graphs discussed in Sec. II. We have seen in Sec. II G that these three-line graphs lead to a three-particle Regge pole at $\alpha_3(\vec{\Delta})$. Therefore, the convolution of this three-particle pole with an elementary particle gives a fixed cut at

$$\zeta = \alpha_3(0) . \tag{3.26}$$

We do not know $\alpha_3(0)$ exactly; however, a more sophisticated variational calculation than that of Sec. II G shows that

$$\alpha_3(0) > 2\alpha(0) . \tag{3.27}$$

Therefore, the "Reggeon-Reggeon" cut is not the right-most branch cut in the $j$ plane.

## IV. COMPARISON WITH GRIBOV'S REGGEON CALCULUS

We have now seen explicitly that in $\phi^3$ theory Mandelstam's diagrams are not nearly enough to study the $s \to \infty$ behavior of the scattering amplitude with either three- or four-particle intermediate states. In the case of three-particle intermediate states, if only Mandelstam's diagrams are taken into account, the amplitude behaves as the convolution of a Reggeon and an elementary particle. In fact, due to the non-Mandelstam diagrams the discontinuity across the cut starting at $j=-2+\alpha(0)$ is different from that given by the Reggeon-particle convolution and, in addition, there is at least one pole that lies to the right of $-2+\alpha(0)$ if $\vec{\Delta}$ is not too large. Moreover, in the case of four-particle intermediate states, the branch point is not at $-3+2\alpha(\vec{\Delta}/2)$ but is at a larger value. In this case, the discontinuity across the branch cut is of course also different from that of the simple convolution of two Regge poles obtained by summing only the double Mandelstam diagrams.

As presented in Sec. II (and III) each of the 3 (or 4) particles in the $t$ channel are treated on an equal footing as is natural and as required by Bose statistics. This leads to an amplitude determined through an integral equation which describes the mutual interaction of the 3 (or 4) particles in the space of transverse momenta. However, it is also possible to proceed in a somewhat different fashion by first summing over the repeated interactions between pairs to produce Reggeons. We discuss here four points of view in connection with this approach.

(a). The calculations of the preceding sections demonstrate that these repeated interactions of Reggeons are just as important as the term which contributes to the single two-Reggeon (or Reggeon-particle) term. A great deal of effort has been spent in the past several years in the nonperturbative study of these repeated interactions of Reggeons in the $t$ channel.[19,20] However, most of this work deals with systems having a triple-Regge vertex. From Sec. II and III here, we find no triple-Regge vertex in the $\phi^3$ problem under consideration, but find instead a four-Regge vertex describing the scattering of two Reggeons to two Reggeons. Furthermore, even in the weak coupling limit and to the leading logarithm approximation, this four-Regge vertex must be taken into account. A four-Regge vertex has been considered before in a nonperturbative fashion,[19] but the theory presented there would also seem to allow the coupling of 1 Reggeon to 3 Reggeons which is not relevant to the present $\phi^3$ problem. A further detailed investigation to clarify the situation would seem desirable.

(b) One can attempt to be more phenomenological and say that we should now multiply the Mandelstam discontinuity formula by some new function in order to get the correct discontinuity. The hope may be realized that, at least when no additional poles appear, this new function is qualitatively simple. To pursue this approach, two lines of attack can be tried. First, on the basis of the diagrams studied in this paper, we may study this ratio of discontinuities, perhaps even numerically. If the result is simple and appealing, it may be tried on cases of more physical interest. Secondly, it is very interesting to look for somewhat different versions of $\phi^3$ theory where perhaps no three-particle Regge pole is present. If such cases can be found, it is then possible to learn about the effect of the three-particle Regge pole on the ratio of discontinuities. In particular, can the sign of this ratio change?

(c) One may force the amplitude into the form of the convolution of a Reggeon and a particle (or of 2 Reggeons) at the expense of using much more complicated (and $s$-dependent) vertex functions for the coupling of the external particles to the Reggeon-particle pair or to the two Reggeons. The possible structure of these vertex functions, usuually called $N$, has been discussed by Gribov,

Pomeranchuk, and Ter-Martirosyan[6] and by Gribov.[9] It would be illuminating to apply these formalisms to $\phi^3$ theory and find out what additional information, if any, need be added to regain the results of Secs. II and III.

(d) Finally, we may argue that $\phi^3$ theory has no relevance to hadron physics. In some sense this is surely correct. However, our $\phi^3$ calculations are for processes where only 3 or 4 particles are exchanged in the $t$ channel. Reggeon calculus would seem to be not inapplicable to such processes. Therefore the usual objection to $\phi^3$ theory about the instability of a system of attractive bosons against collapse is perhaps not a serious source of difficulty.

On the other hand, $\phi^3$ theory in the weak coupling limit suffers unavoidably from the problem that the Born approximation is larger than the single-Reggeon (ladder) approximation by a power of $s$ and that the diagrams with 3 particles in the $t$ channel are down from ladder graphs by another power of $s$. The renders discussion of the relation of $\phi^3$ to Reggeon calculus somewhat uncertain. To overcome this problem a systematic study of some other field theory is essential. The most natural candidate is perhaps quantum electrodynamics.


## ACKNOWLEDGMENTS

We are pleased to acknowledge helpful discussions with Professor B. W. Lee and Dr. A. R. White. We are grateful to Professor O. J. Kleppa, Professor K. W. Schwarz, and Professor B. W. Lee for their hospitality at the James Franck Institute of the University of Chicago and the Fermi National Accelerator Laboratory, where this research was carried out on alternate days.


## APPENDIX A

The following integral appears repeatedly in the Mellin transform of both Mandelstam and non-Mandelstam amplitudes

$$I=\int_{-x_1}^{x_2}dx\int_{-y_1}^{y_2}dy\,(xy+a+i\epsilon)^{-p}, \tag{A1}$$

where $\mathrm{Re}p>1$, and $x_1$, $x_2$, $y_1$, and $y_2$ are all fixed positive numbers. We want to evaluate $I$ approximately for small $a$.

Integration over $y$ gives

$$I=-(p-1)^{-1}\int_{-x_1}^{x_2}dx\,x^{-1}[(xy_2+a+i\epsilon)^{-p+1}-(-xy_1+a+i\epsilon)^{-p+1}]. \tag{A2}$$

Since the corresponding integrations over $(-\infty,-x_1)$ and $(x_2,\infty)$ are both bounded as $a\to 0$, we get from (A2)

$$I=-(p-1)^{-1}\int_{-\infty}^{\infty}dx\,(x+i\epsilon)^{-1}[(xy_2+a+i\epsilon)^{-p+1}-(-xy_1+a+i\epsilon)^{-p+1}]+O(1). \tag{A3}$$

Here the integral of the first term vanishes by closing the contour in the upper half plane, while the second term gives

$$I=-2\pi i(p-1)^{-1}(a+i\epsilon)^{-p+1}+O(1) \tag{A4}$$

as $a\to 0$. The larger $\mathrm{Re}p$ is, the smaller the relative error becomes.

## APPENDIX B

In this appendix we study the behavior, as $s\to\infty$ with fixed $t$, of the tenth-order Feynman diagram of Fig. 2(a). This is the lowest-order non-Mandelstam diagram that we need to consider. This diagram is redrawn in Fig. 15 in a more symmetrical fashion. Our asymptotic evaluation will be carried out by means of Feynman parameters.

The amplitude for this diagram is

$$\mathfrak{M}_1^{(10)}=-4!\,(16\pi^2)^{-4}g^{10}\mathfrak{g}_1^{(10)}, \tag{B1}$$

where

$$\mathfrak{g}_1^{(10)}=\int_0^1 d\{\alpha\}\,\frac{\Lambda^3\delta(\sum\alpha-1)}{(sD_s+uD_u+tD_t-m^2D_m+i\epsilon)^5}\,. \tag{B2}$$

In (B2), $\alpha$ stands symbolically for all the Feynman parameters, including all the $\alpha$, $\alpha'$, $\beta$, $\beta'$, and $\gamma$ of Fig. 15. As $s\to\infty$ with fixed $t$, $u$ is approximately $-s$; hence the coefficient of $s$ is $D_s-D_u$.

In (B2), $\Lambda$, $D_s$, $D_u$, $D_t$, and $D_m$ are functions of all the $\alpha$'s. They can be described in a number of

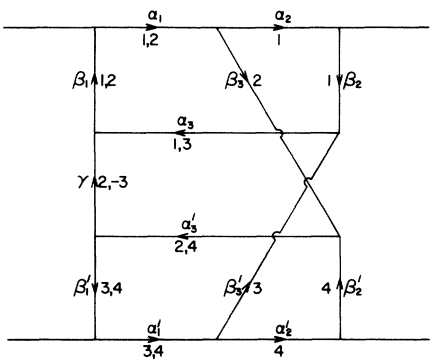


FIG. 15. The Feynman diagram studied in Appendix B.

ways. For example, $\Lambda$ is given by the sum of all the cuts that leave the diagram connected, where $D_s$, $D_u$, and $D_t$ are respectively the sum of all the cuts in the $s$, $u$, and $t$ channels.[26] We find it convenient to use instead the determinantal form originally given by Chisolm.[27] In fact, for some of the more complicated diagrams to be treated in later appendixes, we have not been able to carry through the analysis in any other way.

The determinants are in fact those from circuit analysis. We begin by choosing independent loop currents. For the diagram of Fig. 15, there are four such loops, indicated by "1," "2," "3," and "4" in the figure. If any loop current in a line is in the direction opposite to the arrow for the line, then we add a minus sign in front of the number for the loop current. Treating the Feynman parameters as resistances, we can write down from circuit analysis the $4\times4$ matrix, where the diagonal element $\lambda_{jj}$ is the sum of all the Feynman parameters in the $j$th loop, while the off-diagonal element $\lambda_{jk}$ is the sum of all the Feynman parameters common to the $j$th and $k$th loops (with a minus sign if the loop currents are in opposite directions). The determinant of this matrix gives $\Lambda$.

To obtain $D_s - D_u$, we add an extra row and an extra column (column 5) to the above $4\times4$ matrix. The (5,5) element is zero, the $(j,5)$ element is the sum of the Feynman parameters in the $j$th loop which are also in the top line of the diagram, and the $(5,j)$ element is the corresponding sum using the bottom line of the diagram. Note that the arrows in the top and bottom lines are both from left to right. $D_s - D_u$ is given by the determinant of this $5\times5$ matrix:

$$D_s - D_u = \begin{vmatrix} \alpha_1+\alpha_2+\alpha_3+\beta_1+\beta_2 & \alpha_1+\beta_1 & \alpha_3 & 0 & \alpha_1+\alpha_2 \\ \alpha_1+\beta_1 & \alpha_1+\alpha_3'+\beta_1+\beta_3+\gamma & -\gamma & \alpha_3' & \alpha_1 \\ \alpha_3 & -\gamma & \alpha_1'+\alpha_3+\beta_1'+\beta_3'+\gamma & \alpha_1'+\beta_1' & 0 \\ 0 & \alpha_3' & \alpha_1'+\beta_1' & \alpha_1'+\alpha_2'+\alpha_3'+\beta_1'+\beta_2' & 0 \\ 0 & 0 & \alpha_1' & \alpha_1'+\alpha_2' & 0 \end{vmatrix}. \tag{B3}$$

We shall not write down $D_t$ and $D_m$ at this stage because they are not needed in their full form. We merely note that they are not zero even if we put all the $\alpha$ and $\alpha'$ to zero.

As a first step, we subtract column 5 from column 1, and subtract row 5 from row 4. Thus

$$D_s - D_u = \begin{vmatrix} \alpha_3+\beta_1+\beta_2 & \alpha_1+\beta_1 & \alpha_3 & 0 & \alpha_1+\alpha_2 \\ \beta_1 & \alpha_1+\alpha_3'+\beta_1+\beta_3+\gamma & -\gamma & \alpha_3' & \alpha_1 \\ \alpha_3 & -\gamma & \alpha_1'+\alpha_3+\beta_1'+\beta_3'+\gamma & \alpha_1'+\beta_1' & 0 \\ 0 & \alpha_3' & \beta_1' & \alpha_3'+\beta_1'+\beta_2' & 0 \\ 0 & 0 & \alpha_1' & \alpha_1'+\alpha_2' & 0 \end{vmatrix}. \tag{B4}$$

We proceed to evaluate this determinant explicitly

$$D_s - D_u = -\gamma(\alpha_1\beta_2 - \alpha_2\beta_1)(\alpha_1'\beta_2' - \alpha_2'\beta_1') + (\alpha_1\beta_2 - \alpha_2\beta_1)\alpha_3'A_1 + (\alpha_1'\beta_2' - \alpha_2'\beta_1')\alpha_3A_2 + \alpha_3\alpha_3'A_3, \tag{B5}$$

where

$$A_1 = (\alpha_3+\beta_3')\alpha_1' + (\alpha_1'+\alpha_3+\beta_1'+\beta_3'+\gamma)\alpha_2', \tag{B6}$$

$$A_2 = (\alpha_3'+\beta_3)\alpha_1 + (\alpha_1+\alpha_3'+\beta_1+\beta_3+\gamma)\alpha_2, \tag{B7}$$

and

$$A_3 = \alpha_1\alpha_1'(\beta_3+\beta_3') - \alpha_2\alpha_2'\gamma + \alpha_1\alpha_2'(\alpha_1'+\beta_1'+\beta_3') + \alpha_1'\alpha_2(\alpha_1+\beta_1+\beta_3). \tag{B8}$$

A more useful form of (B5) is

$$D_s - D_u = -\gamma(\alpha_1\beta_2 - \alpha_2\beta_1 - \alpha_3A_2/\gamma)(\alpha_1'\beta_2' - \alpha_2'\beta_1' - \alpha_3'A_1/\gamma) + \alpha_3\alpha_3'B/\gamma, \tag{B9}$$

where

$$B = A_1 A_2 + \gamma A_3$$

$$= [(\alpha_3 + \beta_3')(\alpha_3' + \beta_3) + \gamma(\beta_3 + \beta_3')]\,\alpha_1\alpha_1' + [(\alpha_1' + \alpha_3 + \beta_1' + \beta_3')(\alpha_1 + \alpha_3' + \beta_1 + \beta_3) + \gamma(\alpha_1 + \alpha_1' + \alpha_3 + \alpha_3' + \beta_1 + \beta_1' + \beta_3 + \beta_3')]\alpha_2\,\alpha_2'$$

$$+ [(\alpha_3' + \beta_3)(\alpha_1' + \alpha_3 + \beta_1' + \beta_3' + \gamma) + \gamma(\alpha_1' + \beta_1' + \beta_3')]\alpha_1\alpha_2' + [(\alpha_3 + \beta_3')(\alpha_1 + \alpha_3' + \beta_1 + \beta_3 + \gamma) + \gamma(\alpha_1 + \beta_1 + \beta_3)]\alpha_1'\alpha_2. \quad \text{(B10)}$$

Since $D_s - D_u$ is the coefficient of $s$ in the denominator of (B2), the most important contribution to $g_1^{(10)}$ comes from the region where $D_s - D_u$ is small. From (B9), $D_s - D_u = 0$ if

$$\alpha_1 = \alpha_2 = 0, \quad \text{(B11)}$$

or

$$\alpha_1' = \alpha_2' = 0, \quad \text{(B12)}$$

or

$$\alpha_1\beta_2 - \alpha_2\beta_1 - \alpha_3 A_2/\gamma = \alpha_3 = 0, \quad \text{(B13)}$$

or

$$\alpha_1\beta_2 - \alpha_2\beta_1 - \alpha_3 A_2/\gamma = \alpha_3' = 0, \quad \text{(B14)}$$

or

$$\alpha_1'\beta_2' - \alpha_2'\beta_1' - \alpha_3' A_1/\gamma = \alpha_3 = 0, \quad \text{(B15)}$$

or

$$\alpha_1'\beta_2' - \alpha_2'\beta_1' - \alpha_3' A_1/\gamma = \alpha_3' = 0. \quad \text{(B16)}$$

The leading contribution comes from, roughly speaking, the region where (B11)–(B16) are simultaneously satisfied. Such cases are conveniently treated by the method of Mellin transform.[28]

Define

$$\bar{g}_1^{(10)}(\zeta) = \int_0^\infty g_1^{(10)} s^{1-\zeta}\, ds. \quad \text{(B17)}$$

Since

$$\int_0^\infty (As + B)^{-n} s^{1-\zeta}\, ds = \frac{\Gamma(2-\zeta)\Gamma(n-2+\zeta)}{(n-1)!} \times A^{-2+\zeta} B^{-n+2-\zeta}, \quad \text{(B18)}$$

we get from (B2) that

$$\bar{g}_1^{(10)}(\zeta) = \frac{\Gamma(2-\zeta)\Gamma(3+\zeta)}{4!} \times \int_0^\infty d\{\alpha\}\Lambda^3\delta(\textstyle\sum\alpha - 1) \times (D_s - D_u + i\epsilon)^{-2+\zeta}(D + i\epsilon)^{-3-\zeta}, \quad \text{(B19)}$$

where

$$D = (4m^2 - t)D_u + tD_t - m^2 D_m. \quad \text{(B20)}$$

In order to get the asymptotic behavior of $g_1^{(10)}$ for large $s$, we need the behavior of $\bar{g}_1^{(10)}(\zeta)$ for small $\zeta$.

In view of (B11) and (B12), let

$$\alpha_1 = \rho\bar{\alpha}_1, \quad \alpha_2 = \rho\bar{\alpha}_2, \quad \text{(B21)}$$

and

$$\alpha_1' = \rho'\bar{\alpha}_1', \quad \alpha_2' = \rho'\bar{\alpha}_2',$$

such that

$$\bar{\alpha}_1 + \bar{\alpha}_2 = \bar{\alpha}_1' + \bar{\alpha}_2' = 1. \quad \text{(B22)}$$

This kind of change of variable is called scaling. Since $\rho$ and $\bar{\rho}$ are small, we can carry out these two integrations to get, for small $\zeta$,

$$\bar{g}_1^{(10)}(\zeta) \sim \tfrac{1}{12}\zeta^{-2} \int_0^1 d\bar{\alpha}_1\, d\bar{\alpha}_2\, d\bar{\alpha}_1'\, d\bar{\alpha}_2'\, d\alpha_3\, d\alpha_3'\, d\beta_1\, d\beta_2\, d\beta_3\, d\beta_1'\, d\beta_2'\, d\beta_3'\, d\gamma\, \delta(1 - \bar{\alpha}_1 - \bar{\alpha}_2)\delta(1 - \bar{\alpha}_1' - \bar{\alpha}_2')$$
$$\times \delta(1 - \alpha_3 - \alpha_3' - \beta_1 - \beta_2 - \beta_3 - \beta_1' - \beta_2' - \beta_3' - \gamma)\Lambda_1^{\,3} D_1^{\,-3}$$
$$\times (-\gamma\{\bar{\alpha}_1\beta_2 - \bar{\alpha}_2\beta_1 - \alpha_3[(\alpha_3' + \beta_3)\bar{\alpha}_1 + (\alpha_3' + \beta_1 + \beta_3 + \gamma)\bar{\alpha}_2]/\gamma\}$$
$$\times \{\bar{\alpha}_1'\beta_2' - \bar{\alpha}_2'\beta_1' - \alpha_3'[(\alpha_3 + \beta_3')\bar{\alpha}_1' + (\alpha_3 + \beta_1' + \beta_3' + \gamma)\bar{\alpha}_2']/\gamma\}$$
$$+ \alpha_3\alpha_3'\{[(\alpha_3 + \beta_3')(\alpha_3' + \beta_3) + \gamma(\beta_3 + \beta_3')]\,\bar{\alpha}_1\bar{\alpha}_1' + [(\alpha_3 + \beta_1' + \beta_3')(\alpha_3' + \beta_1 + \beta_3) + \gamma(\alpha_3 + \alpha_3' + \beta_1 + \beta_1' + \beta_3 + \beta_3')]\,\bar{\alpha}_2\bar{\alpha}_2'$$
$$+ [(\alpha_3' + \beta_3)(\alpha_3 + \beta_1' + \beta_3' + \gamma) + \gamma(\beta_1' + \beta_3')]\,\bar{\alpha}_1\bar{\alpha}_2' + [(\alpha_3 + \beta_3')(\alpha_3' + \beta_1 + \beta_3 + \gamma) + \gamma(\beta_1 + \beta_3)]\bar{\alpha}_1'\bar{\alpha}_2\}/\gamma + i\epsilon)^{-2+\zeta}, \quad \text{(B23)}$$

where

$$\Lambda_1 = \Lambda|_{\alpha_1=\alpha_2=\alpha_1'=\alpha_2'=0}$$

and (B24)

$$D_1 = D|_{\alpha_1=\alpha_2=\alpha_1'=\alpha_2'=0}.$$

If we identify the quantities in the first two braces of the last factor in (B23) with the $x$ and $y$ of Appendix A, i.e.,

$$x = \bar{\alpha}_1\beta_2 - \bar{\alpha}_2\beta_1 - \alpha_3[(\alpha_3'+\beta_3)\bar{\alpha}_1 + (\alpha_3'+\beta_1+\beta_3+\gamma)\bar{\alpha}_2]/\gamma$$

and (B25)

$$y = \bar{\alpha}_1'\beta_2' - \bar{\alpha}_2'\beta_1' - \alpha_3'[(\alpha_3+\beta_3')\bar{\alpha}_1' + (\alpha_3+\beta_1'+\beta_3'+\gamma)\bar{\alpha}_2']/\gamma,$$

then we get from (A4) that

$$\begin{aligned}\bar{g}_1^{(10)}(\zeta) \sim -\tfrac{1}{6}\pi i\zeta^{-2}\int_0^1 d\alpha_3\, d\alpha_3'\, d\beta_1\, d\beta_2\, d\beta_3\, d\beta_1'\, d\beta_2'\, d\beta_3'\, d\gamma\, \delta(1-\alpha_3-\alpha_3'-\beta_1-\beta_2-\beta_3-\beta_1'-\beta_2'-\beta_3'-\gamma)\Lambda_1{}^3(D_1+i\epsilon)^{-3}\gamma^{-1}\\ \times[\beta_1+\beta_2+\alpha_3(\beta_1+\gamma)/\gamma]^{-1}[\beta_1'+\beta_2'+\alpha_3'(\beta_1'+\gamma)/\gamma]^{-1}\\ \times\{\alpha_3\alpha_3'\gamma^{-1}\{[(\alpha_3+\beta_3')(\alpha_3'+\beta_3)+\gamma(\beta_3+\beta_3')]\bar{\alpha}_{10}\bar{\alpha}_{10}' + [(\alpha_3+\beta_1'+\beta_3')(\alpha_3'+\beta_1+\beta_3)\\ +\gamma(\alpha_3+\alpha_3'+\beta_1+\beta_1'+\beta_3+\beta_3')]\bar{\alpha}_{20}\bar{\alpha}_{20}'\\ +[(\alpha_3'+\beta_3)(\alpha_3+\beta_1'+\beta_3'+\gamma)+\gamma(\beta_1'+\beta_3')]\bar{\alpha}_{10}\bar{\alpha}_{20}'\\ +[(\alpha_3+\beta_3')(\alpha_3'+\beta_1+\beta_3+\gamma)+\gamma(\beta_1+\beta_3)]\bar{\alpha}_{10}'\bar{\alpha}_{20}\}+i\epsilon)^{-1+\zeta},\end{aligned} \tag{B26}$$

where $\bar{\alpha}_{10}$, $\bar{\alpha}_{20}$, $\bar{\alpha}_{10}'$, and $\bar{\alpha}_{20}'$ are obtained from (B22) and (B25) with $x=y=0$.

It is now clear that the leading behavior of $\bar{g}_1^{(10)}(\zeta)$ for $\zeta$ small is from $\alpha_3 \sim \alpha_3' \sim 0$. Thus

$$\begin{aligned}\bar{g}_1^{(10)}(\zeta) \sim -\tfrac{1}{6}\pi i\zeta^{-4}\int_0^1 d\beta_1\, d\beta_2\, d\beta_3\, d\beta_1'\, d\beta_2'\, d\beta_3'\, d\gamma\, \delta(1-\beta_1-\beta_2-\beta_3-\beta_1'-\beta_2'-\beta_3'-\gamma)\Lambda_0{}^3 D_0{}^{-3}\\ \times\{[\beta_3\beta_3'+\gamma(\beta_3+\beta_3')]\beta_1\beta_1' + [(\beta_1'+\beta_3')(\beta_1+\beta_3)+\gamma(\beta_1+\beta_1'+\beta_3+\beta_3')]\beta_2\beta_2'\\ +[\beta_3(\beta_1'+\beta_3'+\gamma)+\gamma(\beta_1'+\beta_3')]\beta_1\beta_2' + [\beta_3'(\beta_1+\beta_3+\gamma)+\gamma(\beta_1+\beta_3)]\beta_1'\beta_2\}^{-1},\end{aligned} \tag{B27}$$

where

$$\Lambda_0 = \Lambda_1|_{\alpha_3=\alpha_3'=0}$$

and (B28)

$$D_0 = D_1|_{\alpha_3=\alpha_3'=0}.$$

Explicitly

$$\Lambda_0 = \begin{vmatrix} \beta_1+\beta_2 & \beta_1 & 0 & 0 \\ \beta_1 & \beta_1+\beta_3+\gamma & -\gamma & 0 \\ 0 & -\gamma & \beta_1'+\beta_3'+\gamma & \beta_1' \\ 0 & 0 & \beta_1' & \beta_1'+\beta_2' \end{vmatrix}$$

= the quantity in the curly brackets of (B27), (B29)

and

$$\begin{aligned}D_0 = t\{&\beta_1\beta_2\beta_3(\beta_1'\beta_2'+\beta_2'\beta_3'+\beta_3'\beta_1') + \beta_1'\beta_2'\beta_3'(\beta_1\beta_2+\beta_2\beta_3+\beta_3\beta_1)\\ &+\gamma[\beta_3\beta_3'(\beta_1+\beta_2)(\beta_1'+\beta_2') + \beta_1\beta_2\beta_3(\beta_1'+\beta_2') + \beta_1'\beta_2'\beta_3'(\beta_1+\beta_2) + \beta_1\beta_2\beta_1'\beta_2']\}\\ &-m^2\Lambda_0.\end{aligned} \tag{B30}$$

The desired asymptotic behavior of $g_1^{(10)}$ then follows from (B27) and (B17) as

$$g_1^{(10)} \sim -\tfrac{1}{36}\pi i s^{-2}(\ln s)^3\int_0^1 d\beta_1\, d\beta_2\, d\beta_3\, d\beta_1'\, d\beta_2'\, d\beta_3'\, d\gamma\, \delta(1-\beta_1-\beta_2-\beta_3-\beta_1'-\beta_2'-\beta_3'-\gamma)\Lambda_0{}^2 D_0{}^{-3}. \tag{B31}$$

When rewritten in terms of momentum integrals, (B31) with (B1) gives (2.7).

The derivation of (B31) is somewhat tedious although straightforward, Let us add the following remarks to clarify the situation.

(a) The leading contribution comes from the pinch singularity

$$x = y = 0, \tag{B32}$$

as given by (B25), together with the end-point singularity

$$\alpha_1 = \alpha_2 = \alpha_3 = \alpha_1' = \alpha_2' = \alpha_3' = 0. \tag{B33}$$

(b) Even for this relatively simple case, the formulas involved are quite lengthy. Since the corresponding formulas for more complicated diagrams are not manageable, we develop in Appendix C a better formalism where, instead of direct expansion, properties of determinants are used. Since the machinery for this formalism is fairly complicated, we have avoided using it here.

(c) Without additional work, what can we say about terms of the order $s^{-2}(\ln s)^2$ in $g_1^{(10)}$? In terms of Mellin transform, we have to deal with terms of order $\zeta^{-3}$. They can come from, for example, the expansion of the factor $\Gamma(2-\zeta)\Gamma(3+\zeta)$, or from the region of large $\rho$, or large $\rho'$, or large $\alpha_3$. All these contributions have the property that the coefficient of $\zeta^{-3}$, when divided by the coefficient of $\zeta^{-4}$, is real. There is only one way to get a ratio that is not real, namely from the last factor of (B19)

$$(D + i\epsilon)^{-3-\zeta}.$$

We see from (B30) that for physical values of momentum transfers $t<0$ and hence $D_0<0$. We therefore get a factor $e^{-i\pi\zeta}$. Therefore (B31) can be improved to be

$$g_1^{(10)} \sim -\tfrac{1}{36}\pi i s^{-2} \times[(\ln s - i\pi)^3 g_1^{(10)} + \text{const}\times(\ln s)^2 + O(\ln s)], \tag{B34}$$

where $g_1^{(10)}$ is the integral over $\beta$, $\beta'$, and $\gamma$ that appears in (B31), and the constant is purely real. Equation (2.7′) follows from (B34).

(d) What does the present consideration say about the crossed diagram shown in Fig. 4(b)? Let us define a corresponding $g_{1c}^{(10)}$, then

$$g_{1c}^{(10)} = g_1^{(10)}|_{s\to u}. \tag{B35}$$

Therefore the Mellin transforms are related by

$$\bar{g}_{1c}^{(10)} \sim \bar{g}_1^{(10)}|_{D_s - D_u \to -(D_s - D_u)}. \tag{B36}$$

We see from (B19) that this change of sign has two effects: a cancellation of the factor $e^{-i\pi\zeta}$ discussed in the last paragraph, and a complex conjugation to restore the signs of $i\epsilon$. Therefore, by (B34)

$$g_{1c}^{(10)} \sim \tfrac{1}{36}\pi i s^{-2} \times[(\ln s)^3 g_1^{(10)} + \text{const}\times(\ln s)^2 + O(\ln s)]. \tag{B37}$$

Since the constants in (B34) and (B37) are the same, we get finally

$$g_1^{(10)} + g_{1c}^{(10)} \sim -\tfrac{1}{12}\pi^2 s^{-2}(\ln s)^2 g_1^{(10)}. \tag{B38}$$

## APPENDIX C

In this appendix we study the behavior, again for $s\to\infty$ with fixed $t$, of the twelfth-order Feynman diagram of Fig. 2(b). The amplitude for this diagram is

$$\mathfrak{M}_1^{(12)} = 5!(16\pi^2)^{-5} g^{12} g_1^{(12)}, \tag{C1}$$

where

$$g_1^{(12)} = \int_0^1 d\{\alpha\} \frac{\Lambda^4 \delta(\sum\alpha - 1)}{(sD_s + uD_u + tD_t - m^2 D_m + i\epsilon)^6}. \tag{C2}$$

Figure 2(b) is redrawn as Fig. 16, where the Feynman parameters and the choice of loop currents are also shown.

Since there are five loop currents, we need to write down a $6\times 6$ determinant for $D_s - D_u$,

$$D_s - D_u = \begin{vmatrix} \alpha_1+\alpha_2+\alpha_3+\beta_1+\beta_2 & \alpha_1+\beta_1 & -\alpha_3 & 0 & 0 & \alpha_1+\alpha_2 \\ \alpha_1+\beta_1 & \alpha_1+\alpha+\beta_1+\beta_3+\beta_4 & \alpha+\beta_4 & \alpha & 0 & \alpha_1 \\ -\alpha_3 & \alpha+\beta_4 & \alpha_3+\alpha_3'+\alpha+\beta_4+\beta_4'+\gamma & \alpha+\beta_4' & -\alpha_3' & 0 \\ 0 & \alpha & \alpha+\beta_4' & \alpha_1'+\alpha+\beta_1'+\beta_3'+\beta_4' & \alpha_1'+\beta_1' & 0 \\ 0 & 0 & -\alpha_3' & \alpha_1'+\beta_1' & \alpha_1'+\alpha_2'+\alpha+\beta_1'+\beta_2' & 0 \\ 0 & 0 & 0 & \alpha_1' & \alpha_1'+\alpha_2' & 0 \end{vmatrix}.$$

The prescription for writing down this determinant is exactly the one used in Appendix B. Once more we subtract the sixth row from the fifth row and the sixth column from the first column to get

$$D_s - D_u = \begin{vmatrix} \alpha_3+\beta_1+\beta_2 & \alpha_1+\beta_1 & -\alpha_3 & 0 & 0 & \alpha_1+\alpha_2 \\ \beta_1 & \alpha_1+\alpha+\beta_1+\beta_3+\beta_4 & \alpha+\beta_4 & \alpha & 0 & \alpha_1 \\ -\alpha_3 & \alpha+\beta_4 & \alpha_3+\alpha_3'+\alpha+\beta_4+\beta_4'+\gamma & \alpha+\beta_4' & -\alpha_3' & 0 \\ 0 & \alpha & \alpha+\beta_4' & \alpha_1'+\alpha+\beta_1'+\beta_3'+\beta_4' & \alpha_1'+\beta_1' & 0 \\ 0 & 0 & -\alpha_3' & \beta_1' & \alpha+\beta_1'+\beta_2' & 0 \\ 0 & 0 & 0 & \alpha_1' & \alpha_1'+\alpha_2' & 0 \end{vmatrix} . \tag{C4}$$

This is the determinant that we shall concentrate on.

What we need is a procedure that can be generalized to deal with more complicated cases. For this purpose, we introduce the following notation: $\mathfrak{D}_{a_1 \cdots a_n, b_1 \cdots b_n}$ means the minor obtained from the right-hand side of (C4) by omitting the $n$ rows $a_1, a_2, a_3, \ldots, a_n$ and the $n$ columns $b_1, b_2, b_3, \ldots, b_n$. Thus for example

$$\mathfrak{D}_{56,45} = \begin{vmatrix} \alpha_3+\beta_1+\beta_2 & \alpha_1+\beta_1 & -\alpha_3 & \alpha_1+\alpha_2 \\ \beta_1 & \alpha_1+\alpha+\beta_1+\beta_3+\beta_4 & \alpha+\beta_4 & \alpha_1 \\ -\alpha_3 & \alpha+\beta_4 & \alpha_3+\alpha_3'+\alpha+\beta_4+\beta_4'+\gamma & 0 \\ 0 & \alpha & \alpha+\beta_4' & 0 \end{vmatrix} , \tag{C5}$$

$$\mathfrak{D}_{12,16} = \begin{vmatrix} \alpha+\beta_4 & \alpha_3+\alpha_3'+\alpha+\beta_4+\beta_4'+\gamma & \alpha+\beta_4' & -\alpha_3' \\ \alpha & \alpha+\beta_4' & \alpha_1'+\alpha+\beta_1'+\beta_3'+\beta_4' & \alpha_1'+\beta_1' \\ 0 & -\alpha_3' & \beta_1' & \alpha+\beta_1'+\beta_2' \\ 0 & 0 & \alpha_1' & \alpha_1'+\alpha_2' \end{vmatrix} , \tag{C6}$$

and

$$\mathfrak{D}_{1256,1456} = \begin{vmatrix} \alpha+\beta_4 & \alpha_3+\alpha_3'+\alpha+\beta_4+\beta_4'+\gamma \\ \alpha & \alpha+\beta_4' \end{vmatrix} . \tag{C7}$$

It is also convenient to use the special notation that $\Omega$ is the determinant with the last row and the last column omitted:

$$\Omega = \mathfrak{D}_{66} . \tag{C8}$$

Furthermore, let $\Omega_{a_1 \cdots a_n, b_1 \cdots b_n}$ denote the corresponding minor obtained from $\Omega$:

$$\Omega_{a_1 \cdots a_n, b_1 \cdots b_n} = \mathfrak{D}_{a_1 \cdots a_n 6, b_1 \cdots b_n 6} . \tag{C9}$$

We are now ready to study $D_s - D_u$ on the basis of (C4). Consider

$$\bar{\delta} = (D_s - D_u)\mathfrak{D}_{1256,1456} - \mathfrak{D}_{56,45}\mathfrak{D}_{12,16} . \tag{C10}$$

Let us consider this $\bar{\delta}$ in three special cases. First, suppose we replace the (3.1) element

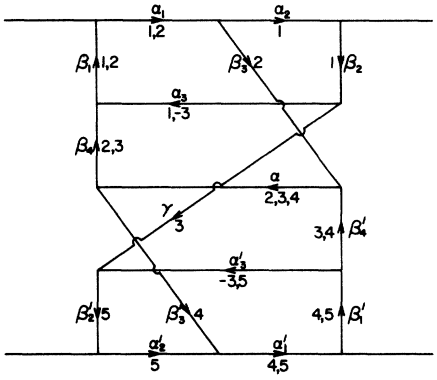


FIG. 16. The Feynman diagram studied in Appendix C.

(which is $-\alpha_3$) of the determinant in (C4) by zero. Then

$$D_s - D_u = \mathfrak{D}_{3456,2345}\mathfrak{D}_{12,16}\,, \tag{C11}$$

$$\mathfrak{D}_{56,45} = \mathfrak{D}_{3456,2345}\mathfrak{D}_{1256,1456}\,, \tag{C12}$$

and hence

$$\bar{\delta} = 0\,. \tag{C13}$$

Secondly, suppose we replace instead the (5, 3) element (which is $-\alpha_3'$) by zero; then

$$D_s - D_u = \mathfrak{D}_{1234,1236}\mathfrak{D}_{56,45}\,, \tag{C14}$$

$$\mathfrak{D}_{12,16} = \mathfrak{D}_{1234,1236}\mathfrak{D}_{1256,1456}\,, \tag{C15}$$

and we again get (C13). Thirdly, suppose we replace the (4, 2) element (which is $\alpha$) by zero, then

$$D_s - D_u = -\mathfrak{D}_{123,126}\mathfrak{D}_{456,345}\,, \tag{C16}$$

$$\mathfrak{D}_{12,16} = \mathfrak{D}_{12456,13456}\mathfrak{D}_{123,126}\,, \tag{C17}$$

$$\mathfrak{D}_{56,45} = -\mathfrak{D}_{12356,12456}\mathfrak{D}_{456,345}\,, \tag{C18}$$

$$\mathfrak{D}_{3456,2345} = \mathfrak{D}_{12456,13456}\mathfrak{D}_{12356,12456}\,, \tag{C19}$$

and we get (C13) once more. Since $\bar{\delta}$ is zero in all these three special cases, $\bar{\delta}$ is in general of the form

$$\bar{\delta} = \alpha_3\alpha_3'\alpha\delta\,, \tag{C20}$$

and

$$D_s - D_u = (\mathfrak{D}_{1256,1456})^{-1}(\mathfrak{D}_{56,45}\mathfrak{D}_{12,16} + \alpha_3\alpha_3'\alpha\delta)\,. \tag{C21}$$

With (C21), we are ready to discuss the behavior, near $\zeta = 0$, of the Mellin transform of the amplitude

$$\begin{aligned}\bar{g}_1^{(12)}(\zeta) &= \int_0^\infty g_1^{(12)} s^{1-\zeta} ds \\ &= \frac{\Gamma(2-\zeta)\Gamma(4+\zeta)}{5!} \\ &\quad \times \int_0^1 d\{\alpha\}\,\Lambda^4\delta(\textstyle\sum\alpha - 1) \\ &\quad \times (D_s - D_u + i\epsilon)^{-2+\zeta}(D + i\epsilon)^{-4-\zeta}\,,\end{aligned} \tag{C22}$$

where $D$ is given by (B20) with the $D_u$, $D_t$, and $D_m$ for the present diagram. Since $D_s - D_u = 0$ if wither $\alpha_1 = \alpha_2 = 0$ or $\alpha_1' = \alpha_2' = 0$, we use the change of variables (B21) and (B22), and first integrate over $\rho$ and $\rho'$:

$$\begin{aligned}\bar{g}_1^{(12)}(\zeta) \sim \tfrac{1}{20}\zeta^{-2}\int_0^1 &d\bar{\alpha}_1 d\bar{\alpha}_2 d\bar{\alpha}_1' d\bar{\alpha}_2' d\alpha_3 d\alpha_3' d\alpha\, d\beta_1 d\beta_2 d\beta_3 d\beta_4 d\beta_1' d\beta_2' d\beta_3' d\beta_4' d\gamma\, \delta(1-\bar{\alpha}_1-\bar{\alpha}_2)\delta(1-\bar{\alpha}_1'-\bar{\alpha}_2') \\ &\times \delta(1-\alpha_3-\alpha_3'-\alpha-\beta_1-\beta_2-\beta_3-\beta_4-\beta_1'-\beta_2'-\beta_3'-\beta_4'-\gamma)\Lambda_1^4(D_1+i\epsilon)^{-4-\zeta}[(D_s-D_u)_1+i\epsilon]^{-2+\zeta}\,,\end{aligned} \tag{C23}$$

where the subscript 1 means the following:

$$\Lambda_1 = \Lambda|_{\alpha_1=\alpha_2=\alpha_1'=\alpha_2'=0}\,, \tag{C24}$$

$$D_1 = D|_{\alpha_1=\alpha_2=\alpha_1'=\alpha_2'=0}\,, \tag{C25}$$

and

$$(D_s - D_u)_1 = \lim_{\rho\to 0,\ \rho'\to 0}(\rho\rho')^{-1}(D_s - D_u)\,. \tag{C26}$$

The second step is to define

$$x = \lim_{\rho\to 0}\rho^{-1}\mathfrak{D}_{56,45}/\mathfrak{D}_{1256,1456} \tag{C27}$$

and

$$y = \lim_{\rho'\to 0}\rho'^{-1}\mathfrak{D}_{12,16}/\mathfrak{D}_{1256,1456}\,, \tag{C28}$$

integrate over $\bar{\alpha}_1$ and $\bar{\alpha}_1'$ by (A4), and then integrate over $\alpha_3$, $\alpha_3'$, and $\alpha$:

$$\begin{aligned}\bar{g}_1^{(12)}(\zeta) \sim -\tfrac{1}{10}\pi i\zeta^{-5}\int_0^1 &d\beta_1 d\beta_2 d\beta_3 d\beta_4 d\beta_1' d\beta_2' d\beta_3' d\beta_4' d\gamma\,(\beta_1+\beta_2)^{-1}(\beta_1'+\beta_2')^{-1}\delta(1-\beta_1-\beta_2-\beta_3-\beta_4-\beta_1'-\beta_2'-\beta_3'-\beta_4'-\gamma) \\ &\times \Lambda_0^4(D_0+i\epsilon)^{-4-\zeta}(\delta_0+i\epsilon)^{-1+\zeta}\,,\end{aligned} \tag{C29}$$

where

$$\begin{aligned}\Lambda_0 &= \Lambda|_{\alpha_1=\alpha_2=\alpha_3=\alpha_1'=\alpha_2'=\alpha_3'=\alpha=0}\,, \\ D_0 &= D|_{\alpha_1=\alpha_2=\alpha_3=\alpha_1'=\alpha_2'=\alpha_3'=\alpha=0}\,,\end{aligned} \tag{C30}$$

and

$$\delta_0 = \left[\lim_{\rho\to 0,\ \rho'\to 0}(\rho\rho')^{-1}\delta\right]^A\,. \tag{C31}$$

In (C31), the superscript $A$ means that the quantity is evaluated at

$$\begin{aligned}\bar{\alpha}_1 &= \beta_1/(\beta_1+\beta_2)\,, \\ \bar{\alpha}_1' &= \beta_1'/(\beta_1'+\beta_2')\,,\end{aligned} \tag{C32}$$

and

$$\alpha_3 = \alpha_3' = \alpha = 0 . \tag{C33}$$

Also note that, in writing down (C29), we have made use of the fact that

$$\mathfrak{D}_{1256,1456}|_{\alpha_3=\alpha_3'=\alpha=0} > 0 . \tag{C34}$$

It remains to find $\delta_0$. For this purpose, some matrix manipulation is necessary:

$$\begin{aligned}
\delta_0 &= \Big[\alpha^{-1} \lim_{\rho\to 0,\ \rho'\to 0} (\rho\rho')^{-1}(\mathfrak{D}_{1256,1456}\mathfrak{D}_{35,13} \\
&\qquad + \mathfrak{D}_{356,145}\mathfrak{D}_{125,136})\Big]^4 \\
&= (\beta_1+\beta_2)^{-1}(\beta_1'+\beta_2')^{-1} \\
&\quad \times [\alpha^{-1}(-\mathfrak{D}_{1256,1456}\mathfrak{D}_{36,36} + \mathfrak{D}_{356,456}\mathfrak{D}_{126,136})]_0 \\
&= (\beta_1+\beta_2)^{-1}(\beta_1'+\beta_2')^{-1} \\
&\quad \times [\alpha^{-1}(\Omega_{35,45}\Omega_{12,13} - \Omega_{125,145}\Omega_{3,3})]_0 \\
&= (\beta_1+\beta_2)^{-2}(\beta_1'+\beta_2')^{-2} \\
&\quad \times [\alpha^{-1}(\Omega_{3,4}\Omega_{2,3} - \Omega_{2,4}\Omega_{3,3})]_0 ,
\end{aligned} \tag{C35}$$

where the subscript 0 means $\alpha_1=\alpha_2=\alpha_3=\alpha_1'=\alpha_2'=\alpha_3'=\alpha=0$. At this stage, we can use Jacobi's identity for minors[29]

$$\Omega_{i,j}\Omega_{k,l} - \Omega_{i,l}\Omega_{k,j} = \Omega\Omega_{ik,jl} \tag{C36}$$

for any determinant $\Omega$, provided that $i<k$ and $j<l$. Therefore

$$\begin{aligned}
\delta_0 &= (\beta_1+\beta_2)^{-2}(\beta_1'+\beta_2')^{-2}(\alpha^{-1}\Omega\Omega_{23,34})_0 \\
&= (\beta_1+\beta_2)^{-1}(\beta_1'+\beta_2')^{-1}(\alpha^{-1}\Omega\Omega_{1235,1345})_0 \\
&= (\beta_1+\beta_2)^{-1}(\beta_1'+\beta_2')^{-1}\Lambda_0 .
\end{aligned} \tag{C37}$$

This is the desired formula.

For $t\le 0$,

$$D_0 = -m^2\Lambda_0 + tD_t|_{\alpha_1=\alpha_2=\alpha_3=\alpha_1'=\alpha_2'=\alpha_3'=\alpha=0} \tag{C38}$$

if negative. If we define

$$g_1^{(12)} = \int_0^1 d\beta_1 d\beta_2 d\beta_3 d\beta_4 d\beta_1' d\beta_2' d\beta_3' d\beta_4' d\gamma\, \delta(1-\beta_1-\beta_2-\beta_3-\beta_4-\beta_1'-\beta_2'-\beta_3'-\beta_4'-\gamma)\Lambda_0^3(-D_0)^{-4} , \tag{C39}$$

then

$$\bar{g}_1^{(12)}(\zeta) \sim -\tfrac{1}{10}\pi i \zeta^{-5} e^{-i\pi\zeta} g_1^{(12)} . \tag{C40}$$

This implies that

$$g_1^{(12)} = -\frac{1}{10}\frac{1}{4!}\pi i s^{-2}[(\ln s - i\pi)^4 g_1^{(12)} + \text{const}\times(\ln s)^3 + O(\ln^2 s)] , \tag{C41}$$

where the constant is real.

For the crossed diagram shown in Fig. 2(b), the corresponding $g_{1c}^{(12)}$ is given by

$$g_{1c}^{(12)} = \frac{1}{10}\frac{1}{4!}\pi i s^{-2}[(\ln s)^4 g_1^{(12)} + \text{const}\times(\ln s)^3 + O(\ln^2 s)] , \tag{C42}$$

and hence

$$g_1^{(12)} + g_{1c}^{(12)} = -\frac{1}{10}\frac{1}{3!}\pi^2 s^{-2}[(\ln s)^3 g_1^{(12)} + O(\ln^2 s)] . \tag{C43}$$

Equation (2.12) follows immediately from (C43).

## APPENDIX D

We apply the formalism of Appendix C to the twelfth-order diagram of Fig. 2(c). The amplitude for this diagram is

$$\mathfrak{M}_2^{(12)} = 5!(16\pi^2)^{-5} g^{12} g_2^{(12)} , \tag{D1}$$

where

$$g_2^{(12)} = \int_0^1 d\{\alpha\}\, \frac{\Lambda^4 \delta(\sum\alpha - 1)}{(sD_s + uD_u + tD_t - m^2 D_m + i\epsilon)^6} . \tag{D2}$$

Figure 17 is the same as Fig. 2(c) with the Feynman parameters and loop currents added on.

For this case, similar to (C4), $D_s - D_u$ is given by

$$D_s-D_u=\begin{vmatrix} \alpha_3+\beta_1+\beta_2 & \alpha_1+\beta_1 & -\alpha_3 & 0 & 0 & \alpha_1+\alpha_2 \\ \beta_1 & \alpha_1+\alpha+\beta_1+\beta_3+\beta_4 & \beta_4 & \alpha & 0 & \alpha_1 \\ -\alpha_3 & \beta_4 & \alpha_3+\alpha_3'+\beta_4+\beta_4'+\gamma & -\beta_4' & \alpha_3' & 0 \\ 0 & \alpha & -\beta_4' & \alpha_1'+\alpha+\beta_1'+\beta_3'+\beta_4' & \alpha_1'+\beta_1' & 0 \\ 0 & 0 & \alpha_3' & \beta_1' & \alpha_3'+\beta_1'+\beta_2' & 0 \\ 0 & 0 & 0 & \alpha_1' & \alpha_1'+\alpha_2' & 0 \end{vmatrix} . \tag{D3}$$

Equations (C10)–(C21) and (C24)–(C28) apply here without any modification at all. Equations (C22) and (C23) also hold if $\bar{g}_1^{(12)}$ is replaced by $\bar{g}_2^{(12)}$. However, since (C34) is not satisfied in the present case, (C29) is replaced by

$$\bar{g}_2^{(12)}(\zeta)\sim-\tfrac{1}{10}\pi i\zeta^{-5}\int_0^1 d\beta_1 d\beta_2 d\beta_3 d\beta_4 d\beta_1' d\beta_2' d\beta_3' d\beta_4' d\gamma(\beta_1+\beta_2)^{-1}(\beta_1'+\beta_2')^{-1}\delta(1-\beta_1-\beta_2-\beta_3-\beta_4-\beta_1'-\beta_2'-\beta_3'-\beta_4'-\gamma)$$
$$\times\Lambda_0^4(D_0+i\epsilon)^{-4-\zeta}(-\delta_0+i\epsilon)^{-1+\zeta}, \tag{D4}$$

where $\Lambda_0$, $D_0$, and $\delta_0$ are still given by (C30)–(C32). This minus sign with $\delta_0$ is neatly compensated, because (C35) holds here if the left-hand side is replaced by $-\delta_0$. This change in sign is due to the fact that the (5,3) element of (D3) is $\alpha_3'$, while that of (C4) is $-\alpha_3'$. Therefore, for the present diagram we get

$$-\delta_0=(\beta_1+\beta_3)^{-1}(\beta_1'+\beta_2')^{-1}\Lambda_0 \tag{D5}$$

instead of (C37).

The similarity between the diagram under consideration and that treated in Appendix C goes even further. If we contract all the $\alpha$ and $\alpha'$ in the diagrams of Figs. 16 and 17, the results are identical. Therefore both $\Lambda_0$ and $D_0$ are entirely the same for the two cases, and the right-hand sides of (C29) and (D4) are identical. Therefore

$$\mathfrak{M}_2^{(12)}=\mathfrak{M}_1^{(12)}[1+O((\ln s)^{-1})], \tag{D6}$$

and

$$\mathfrak{M}_2^{(12)}+\mathfrak{M}_{2c}^{(12)}=(\mathfrak{M}_1^{(12)}+\mathfrak{M}_{1c}^{(12)})[1+O((\ln s)^{-1})]. \tag{D7}$$

## APPENDIX E

We next apply the formalism of Appendix C to the twelfth-order diagram of Fig. 2(d). The amplitude for this diagram is

$$\mathfrak{M}_3^{(12)}=5!(16\pi^2)^{-5}g^{12}g_3^{(12)}, \tag{E1}$$

where

$$g_3^{(12)}=\int_0^1 d\{\alpha\}\,\frac{\Lambda^4\delta(\sum\alpha-1)}{(sD_s+uD_u+tD_t-m^2D_m+i\epsilon)^6}\,. \tag{E2}$$

Figure 2(d) has been redrawn as Fig. 18.

For this case, similar to (C4), $D_s-D_u$ is given by

$$D_s-D_u=\begin{vmatrix} \alpha_3+\beta_1+\beta_2 & \alpha_1+\beta_1 & -\alpha_3 & 0 & 0 & \alpha_1+\alpha_2 \\ \beta_1 & \alpha_1+\alpha_3'+\beta_1+\beta_3+\beta_4+\gamma & \beta_4 & -\gamma & \alpha_3' & \alpha_1 \\ -\alpha_3 & \beta_4 & \alpha_3+\alpha+\beta_4+\beta_4' & \alpha & 0 & 0 \\ 0 & -\gamma & \alpha & \alpha_1'+\alpha+\beta_1'+\beta_3'+\gamma & \alpha_1'+\beta_1' & 0 \\ 0 & \alpha_3' & 0 & \beta_1' & \alpha_3'+\beta_1'+\beta_2' & 0 \\ 0 & 0 & 0 & \alpha_1' & \alpha_1'+\alpha_2' & 0 \end{vmatrix} . \tag{E3}$$

Although it is possible to treat this determinant directly, we can save a great deal of writing by interchanging the second and the third columns. Let us add a minus sign to every element of the new third column to get

$$D_s - D_u = \begin{vmatrix} \alpha_3+\beta_1+\beta_2 & -\alpha_3 & -\alpha_1-\beta_1 & 0 & 0 & \alpha_1+\alpha_2 \\ \beta_1 & \beta_4 & -\alpha_1-\alpha_3'-\beta_1-\beta_3-\beta_4-\gamma & -\gamma & \alpha_3' & \alpha_1 \\ -\alpha_3 & \alpha_3+\alpha+\beta_4+\beta_4' & -\beta_4 & \alpha & 0 & 0 \\ 0 & \alpha & \gamma & \alpha_1'+\alpha+\beta_1'+\beta_3'+\gamma & \alpha_1'+\beta_1' & 0 \\ 0 & 0 & -\alpha_3' & \beta_1' & \alpha_3'+\beta_1'+\beta_2' & 0 \\ 0 & 0 & 0 & \alpha_1' & \alpha_1'+\alpha_2' & 0 \end{vmatrix} . \tag{E4}$$

The similarity between (E4) and (C4) is now striking. In particular, the crucial elements at the (3, 1), (4, 2), and (5, 3) positions are identical. Therefore, the entire analysis of Appendix C goes through with no modification. The final results for $g_3^{(12)}$, $g_{3c}^{(12)}$, and their sum are given respectively by the right-hand sides of (C41), (C42), and (C43).

Unlike the previous case of Appendix D, both $D_0$ and $\Lambda_0$ are given by different formulas in the present case than those of Appendix C.

## APPENDIX F

In this appendix, we generalize the method of Appendix C to deal with the Reggeon-Reggeon cut. This generalization is not completely straightforward.

Instead of starting with the non-Mandelstam diagram of the lowest possible order, we prefer to treat here a case of particular interest. Specifically we shall find the asymptotic behavior, for large $s$ and fixed $t$, of the contribution from the Feynman diagram of Fig. 9. This is a twentieth-order diagram, and gives the effect of Reggeon-Reggeon scattering. The matrix element is

$$\mathfrak{M}_1^{(20)} = 9!(16\pi^2)^{-9} g^{20} I_1^{(20)} , \tag{F1}$$

where

$$I_1^{(20)} = \int d\{\alpha\} \frac{\Lambda^8 \delta(\sum\alpha - 1)}{(sD_s + uD_u + tD_t - m^2 D_m + i\epsilon)^{10}} . \tag{F2}$$

This diagram of Fig. 9 is redrawn as Fig. 10.

With the choice of loop currents shown $D_s - D_u$ can be expressed in terms of a $10\times 10$ determinant. Analogous to (C4), after subtracting the tenth column from the first column and the tenth row from the ninth row, the result is

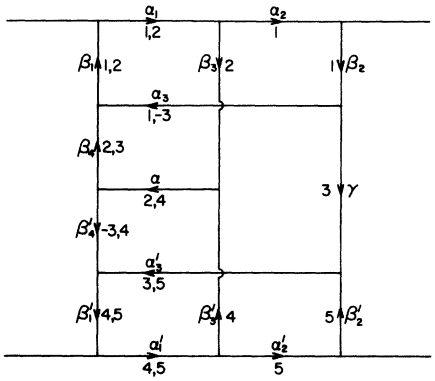


FIG. 17. The Feynman diagram studied in Appendix D.

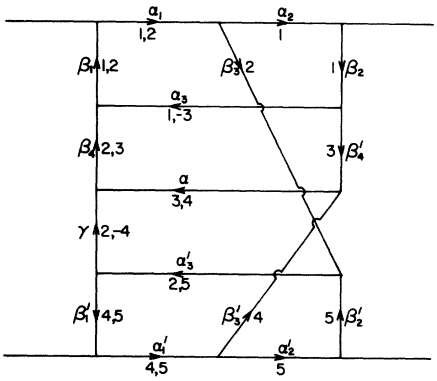


FIG. 18. The Feynman diagram studied in Appendix E.

$$
D_3 - D_4 = \begin{vmatrix}
\alpha_4+\beta_1+\beta_2 & \alpha_3 & -\alpha_4 & \alpha_1+\beta_1 & 0 & 0 & 0 & 0 & 0 & \alpha_1+\alpha_2+\alpha_3 \\
0 & \alpha_3+\alpha_5+\beta_3+\beta_4 & 0 & -\beta_3 & \alpha_5 & 0 & 0 & 0 & 0 & \alpha_3 \\
-\alpha_4 & 0 & \alpha_4+\alpha_6+\beta_5+\beta_6 & \beta_5 & -\alpha_6 & \alpha_6 & 0 & 0 & 0 & 0 \\
\beta_1 & -\beta_3 & \beta_5 & \alpha_1+\alpha_6'+\beta_1+\beta_3+\beta_5+\beta_7+\gamma_1 & \alpha_6'+\beta_7+\gamma_1 & -\gamma_1 & \alpha_6' & 0 & 0 & \alpha_1 \\
0 & \alpha_5 & -\alpha_6 & \alpha_6'+\beta_7+\gamma_1 & \alpha_5+\alpha_5'+\alpha_6+\alpha_6'+\beta_7+\beta_7'+\gamma_1+\gamma_2 & -\alpha_6'-\beta_7'-\gamma_1 & \alpha_6' & -\alpha_5' & 0 & 0 \\
0 & 0 & \alpha_6 & -\gamma_1 & -\alpha_6-\beta_7'-\gamma_1 & \alpha_1'+\alpha_6+\beta_1'+\beta_3'+\beta_5'+\beta_7'+\gamma_1 & \beta_5' & -\beta_3' & \alpha_1'+\beta_1' & 0 \\
0 & 0 & 0 & \alpha_6' & \alpha_6' & \beta_5' & \alpha_4'+\alpha_6'+\beta_5'+\beta_6' & 0 & -\alpha_4' & 0 \\
0 & 0 & 0 & 0 & -\alpha_5' & -\beta_3' & 0 & \alpha_3'+\alpha_5'+\beta_3'+\beta_4' & \alpha_3' & 0 \\
0 & 0 & 0 & 0 & 0 & \beta_1' & -\alpha_4' & 0 & \alpha_4'+\beta_1'+\beta_2' & 0 \\
0 & 0 & 0 & 0 & 0 & \alpha_1' & 0 & \alpha_3' & \alpha_1'+\alpha_2'+\alpha_3' & 0
\end{vmatrix}
\qquad \text{(F3)}
$$

We encounter here the first difference between four-line diagrams and three-line diagrams. The right-hand side of (F3) is zero if one of the following four sets of conditions is satisfied:

$$\alpha_1=\alpha_2=\alpha_3=0, \tag{F4}$$

$$\alpha_4=\beta_1=\beta_2=0, \tag{F5}$$

$$\alpha_1'=\alpha_2'=\alpha_3'=0, \tag{F6}$$

and

$$\alpha_4'=\beta_1'=\beta_2'=0. \tag{F7}$$

However, $\Lambda$, which appears in the numerator of (F2), also vanishes if (F4) and (F5) are both satisfied, or if (F6) and (F7) are both satisfied. Therefore the leading contribution to $I_1^{(20)}$ comes from 4 independent regions in the vicinity of the following points: (1) (F4) and (F6), (2) (F4) and (F7), (3) (F5) and (F6), and (4) (F5) and (F7). These four regions need to be studied separately. For definiteness, we shall treat here only the first region.

Consider the difference

$$\tilde{\delta}=\mathfrak{D}_{1490,1690}(D_s-D_u)-\mathfrak{D}_{90,69}\mathfrak{D}_{14,10}, \tag{F8}$$

where the subscript 0 is used to designate the tenth row or column. Similar to the treatment in Appendix C, we consider two special cases. First, suppose that the (2, 10) element $d_{20}$ (which is equal to $\alpha_3$) and the (3, 1) element $d_{31}$ (which is $-\alpha_4$) of the determinant are both replaced by zero, then we have

$$D_s-D_u=\mathfrak{D}_{23567890,23456789}\mathfrak{D}_{14,10}, \tag{F9}$$

$$\mathfrak{D}_{90,69}=\mathfrak{D}_{23567890,23456789}\mathfrak{D}_{1490,1690}, \tag{F10}$$

and hence

$$\tilde{\delta}=0. \tag{F11}$$

Similarly, when the (10, 8) element $d_{08}$ (which is $\alpha_3'$) and the (9, 7) element $d_{97}$ (which is $-\alpha_4'$) are both replaced by zero, then

$$D_s-D_u=\mathfrak{D}_{12345678,12345780}\mathfrak{D}_{90,69}, \tag{F12}$$

$$\mathfrak{D}_{14,10}=\mathfrak{D}_{12345678,12345780}\mathfrak{D}_{1490,1690}, \tag{F13}$$

and hence we get (F11) again. Thus $\tilde{\delta}$ vanishes when $d_{20}=d_{31}=0$ or $d_{08}=d_{97}=0$. We can therefore expand $\tilde{\delta}$ with respect to these four elements

$$\tilde{\delta}=\tilde{\delta}'+\tilde{\delta}'', \tag{F14}$$

where $\tilde{\delta}'$ is the quadratic part, which is of the form

$$\tilde{\delta}'=d_{20}d_{08}\tilde{\delta}_1+d_{20}d_{97}\tilde{\delta}_2+d_{31}d_{08}\tilde{\delta}_3+d_{31}d_{97}\tilde{\delta}_4, \tag{F15}$$

and $\tilde{\delta}'$ is the cubic and quartic part, which is of the form

$$\tilde{\delta}''=d_{20}d_{31}(d_{08}\tilde{\delta}_5+d_{97}\tilde{\delta}_6)+d_{08}d_{97}(d_{20}\tilde{\delta}_7+d_{31}\tilde{\delta}_8)+d_{20}d_{31}d_{08}d_{97}\tilde{\delta}_9. \tag{F16}$$

These $\tilde{\delta}_i$ can be written down explicitly by direct expansion. Let $\mathfrak{D}'$ have the same meaning as $\mathfrak{D}$ except that the (2, 10), (3, 1), (10, 8), and (9, 7) elements are all set equal to zero. Then

$$\tilde{\delta}_1=-\mathfrak{D}_{1490,1690}\mathfrak{D}'_{20,80}+\mathfrak{D}'_{290,690}\mathfrak{D}'_{140,180}, \tag{F17}$$

$$\tilde{\delta}_2=-\mathfrak{D}_{1490,1690}\mathfrak{D}'_{29,70}+\mathfrak{D}'_{290,690}\mathfrak{D}'_{149,170}, \tag{F18}$$

$$\tilde{\delta}_3=\mathfrak{D}_{1490,1690}\mathfrak{D}'_{30,18}-\mathfrak{D}'_{390,169}\mathfrak{D}'_{140,180}, \tag{F19}$$

and

$$\tilde{\delta}_4=\mathfrak{D}_{1490,1690}\mathfrak{D}'_{39,17}-\mathfrak{D}'_{390,169}\mathfrak{D}'_{149,170}. \tag{F20}$$

Jacobi's identity may be applied to each of these four $\tilde{\delta}$'s to give respectively

$$\tilde{\delta}_1=\mathfrak{D}'_{0,0}\mathfrak{D}'_{12490,16890}, \tag{F21}$$

$$\tilde{\delta}_2=\mathfrak{D}'_{9,0}\mathfrak{D}'_{12490,16790}, \tag{F22}$$

$$\tilde{\delta}_3=\mathfrak{D}'_{0,1}\mathfrak{D}'_{13490,16890}, \tag{F23}$$

$$\tilde{\delta}_4=\mathfrak{D}'_{9,1}\mathfrak{D}'_{13490,16790}. \tag{F24}$$

In order to go further, we consider, corresponding to the pinch singularity, the special case where

$$d_{10}=\mu d_{11},\quad d_{40}=\mu d_{41},\qquad d_{06}=\mu' d_{96},\quad d_{09}=\mu' d_{99}. \tag{F25}$$

Let $\mathfrak{D}''$ be $\mathfrak{D}'$ when (F25) is satisfied,

$$\mathfrak{D}''=\mathfrak{D}'|_{(F25)}, \tag{F26}$$

then

$$\begin{aligned}\mathfrak{D}''_{0,0}&=\mu'^{-1}\mathfrak{D}''_{9,0}\\&=\mu^{-1}\mathfrak{D}''_{0,1}\\&=(\mu\mu')^{-1}\mathfrak{D}''_{9,1},\end{aligned} \tag{F27}$$

and hence

$$\tilde{\delta}'|_{(F25)} = \mathfrak{D}''_{0,0}(d_{20}d_{08}\,\mathfrak{D}'_{12490,16890} + \mu' d_{20}d_{97}\,\mathfrak{D}'_{12490,16790} + \mu d_{31}d_{08}\,\mathfrak{D}'_{13490,16890} + \mu\mu' d_{31}d_{97}\,\mathfrak{D}'_{13490,16790})$$

$$= \mathfrak{D}''_{0,0}\begin{vmatrix}
\alpha_3+\alpha_5+\beta_3+\beta_4 & 0 & -\beta_3 & \alpha_5 & 0 & 0 & \alpha_3 \\
0 & \alpha_4+\alpha_6+\beta_5+\beta_6 & \beta_5 & -\alpha_6 & 0 & 0 & \mu\alpha_4 \\
\alpha_5 & -\alpha_6 & \alpha'_6+\beta_7+\gamma_1 & \alpha_5+\alpha'_5+\alpha_6+\alpha'_6+\beta_7+\beta'_7+\gamma_1+\gamma_2 & \alpha'_6 & -\alpha'_5 & 0 \\
0 & \alpha_6 & -\gamma_1 & -\alpha_6-\beta'_7-\gamma_1 & \beta'_5 & -\beta'_3 & 0 \\
0 & 0 & \alpha'_6 & \alpha'_6 & \alpha'_4+\alpha'_6+\beta'_5+\beta'_6 & 0 & 0 \\
0 & 0 & 0 & -\alpha'_5 & 0 & \alpha'_3+\alpha'_5+\beta'_3+\beta'_4 & 0 \\
0 & 0 & 0 & 0 & \mu'\alpha'_4 & \alpha'_3 & 0
\end{vmatrix}$$

$$= \mathfrak{D}''_{0,0}\Bigg[-\alpha_3\alpha_5\alpha'_3\alpha'_5\begin{vmatrix} \alpha_4+\alpha_6+\beta_5+\beta_6 & \beta_5 & 0 \\ \alpha_6 & -\gamma_1 & \beta'_5 \\ 0 & \alpha'_6 & \alpha'_4+\alpha'_6+\beta'_5+\beta'_6 \end{vmatrix}$$

$$-\mu'\alpha_3\alpha_5\alpha'_4\alpha'_6\begin{vmatrix} \alpha_4+\alpha_6+\beta_5+\beta_6 & -\alpha_6 & 0 \\ \alpha_6 & -\alpha_6-\beta'_7 & -\beta'_3 \\ 0 & -\alpha'_5 & \alpha'_3+\alpha'_5+\beta'_3+\beta'_4 \end{vmatrix}$$

$$+\mu\alpha_4\alpha_6\alpha'_3\alpha'_5\begin{vmatrix} \alpha_3+\alpha_5+\beta_3+\beta_4 & -\beta_3 & 0 \\ \alpha_5 & \alpha'_6+\beta_7 & \alpha'_6+\beta'_5 \\ 0 & \alpha'_6 & \alpha'_4+\alpha'_6+\beta'_5+\beta'_6 \end{vmatrix}$$

$$+\mu\mu'\alpha_4\alpha_6\alpha'_4\alpha'_6\begin{vmatrix} \alpha_3+\alpha_5+\beta_3+\beta_4 & \alpha_5 & 0 \\ \alpha_5 & \alpha_5+\alpha'_5+\gamma_2 & -\alpha'_5-\beta'_3 \\ 0 & -\alpha'_5 & \alpha'_3+\alpha'_5+\beta'_3+\beta'_4 \end{vmatrix}\Bigg] \quad . \tag{F28}$$

After this rather lengthy study of the $s$ coefficient $D_s - D_u$, we are now ready to study the asymptotic behavior of $I_1^{(20)}$ when $s \to \infty$ with fixed $t$. It is convenient to define the Mellin transform slightly differently as

$$\mathcal{I}_1^{(20)}(\zeta) = \int_0^\infty I_1^{(20)} s^{2-\zeta}\, d\zeta \tag{F29}$$

instead of (B17). By (F2)

$$\mathcal{I}_1^{(20)}(\zeta) = \frac{\Gamma(3-\zeta)\Gamma(7+\zeta)}{9!}\int_0^1 d\{\alpha\}\Lambda^8\delta(\textstyle\sum\alpha - 1)(D_s - D_u + i\epsilon)^{-3+\zeta}(D + i\epsilon)^{-7-\zeta}\,, \tag{F30}$$

where $D$ is still defined by (B20). As discussed after (F7), there are four independent regions of contribution. We shall concentrate on region 1, and call the contributions from region 1 to $I_1^{(20)}$ and $\bar{I}_1^{(20)}(\zeta)$, respectively, $I_{1,1}^{(20)}$ and $\mathcal{I}_{1,1}^{(20)}(\zeta)$.

The change of variables (B21) and (B22) is generalized to

$$\alpha_1 = \rho\bar{\alpha}_1,\quad \alpha_2 = \rho\bar{\alpha}_2,\quad \alpha_3 = \rho\bar{\alpha}_3,\quad \alpha'_1 = \rho'\bar{\alpha}'_1,\quad \alpha'_2 = \rho'\bar{\alpha}'_2,\quad \alpha'_3 = \rho'\alpha'_3\,, \tag{F31}$$

and

$$\bar{\alpha}_1 + \bar{\alpha}_2 + \bar{\alpha}_3 = \bar{\alpha}'_1 + \bar{\alpha}'_2 + \bar{\alpha}'_3 = 1\,.$$

For small $\zeta$, we get by carrying out the $\rho$ and $\rho'$ integrations

$$\mathcal{I}_{1,1}^{(20)}(\zeta) \sim \tfrac{1}{252}\,\zeta^{-2}\int_0^1 d\bar{\alpha}\,d\bar{\alpha}'\,d\alpha\,d\alpha'\,d\beta\,d\beta'\,d\gamma\,\delta(1-\textstyle\sum\alpha-\sum\alpha'-\sum\beta-\sum\beta'-\sum\gamma)\delta(1-\sum\bar{\alpha})\delta(1-\sum\bar{\alpha}')$$
$$\times\,\Lambda_1^8(D_1 + i\epsilon)^{-7-\zeta}\left[(D_s - D_u)_1 + i\epsilon\right]^{-3+\zeta}\,, \tag{F32}$$

where

$$d\bar{\alpha} = d\bar{\alpha}_1 d\bar{\alpha}_2 d\bar{\alpha}_3, \qquad d\alpha = d\alpha_4 d\alpha_5 d\alpha_6, \tag{F33}$$

etc. Similar to (C24) and (C25), $D_1$ and $\Lambda_1$ are defined by

$$\Lambda_1 = \Lambda\,|_{\alpha_1=\alpha_2=\alpha_3=\alpha_1'=\alpha_2'=\alpha_3'=0} \tag{F34}$$

and

$$D_1 = D\,|_{\alpha_1=\alpha_2=\alpha_3=\alpha_1'=\alpha_2'=\alpha_3'=0}, \tag{F35}$$

while $(D_s - D_u)_1$ is defined by (C26).

In view of (F8), we define, analogous to (C27) and (28),

$$x = \lim_{\rho\to 0} \rho^{-1}\mathfrak{D}_{90,69}/\mathfrak{D}_{1490,1690} \tag{F36}$$

and

$$y = \lim_{\rho'\to 0} \rho'^{-1}\mathfrak{D}_{14,10}/\mathfrak{D}_{1490,1690}. \tag{F37}$$

Unlike (C34), the above denominator $\mathfrak{D}_{1490,1690}$ does not have a definite sign. We therefore define

$$\lambda = \text{sign of } \mathfrak{D}_{1490,1690}. \tag{F38}$$

Because of (F14)–(F26), $\bar{\alpha}_3$, $\bar{\alpha}_3'$, $\alpha_4$, and $\alpha_4'$ are all small in the important region of integration. Thus $\tilde{\delta}$ may be replaced by $\tilde{\delta}'$ and the integration over $\bar{\alpha}_1$ and $\bar{\alpha}_1'$ gives

$$I^{(20)}_{1,1}(\zeta) \sim -\tfrac{1}{252}\pi i \zeta^{-2} \int d\bar{\alpha}_3 d\bar{\alpha}_3'\, d\alpha\, d\alpha' d\beta\, d\beta' d\gamma\, \delta(1-\textstyle\sum\alpha-\sum\alpha'-\sum\beta-\sum\beta'-\sum\gamma)$$
$$\times |\mathfrak{D}_{1490,1690}|\,(\beta_1+\beta_2)^{-1}(\beta_1'+\beta_2')^{-1}\Lambda_1^{8}(D_1+i\epsilon)^{-7+\zeta}(\lambda\tilde{\delta}_A'+i\epsilon)^{-2+\zeta}, \tag{F39}$$

where

$$\tilde{\delta}_A' = \left[\lim_{\rho\to 0,\,\rho'\to 0}(\rho\rho')^{-1}\tilde{\delta}'\right]^A, \tag{F40}$$

and the superscript $A$ here means (C32) without (C33).

Equation (F28) can now be used to yield

$$I^{(20)}_{1,1}(\zeta) \sim -\tfrac{1}{252}\pi i \zeta^{-2} \int d\bar{\alpha}_3 d\bar{\alpha}_3'\, d\alpha\, d\alpha'\, d\beta\, d\beta'\, d\gamma\, \tilde{\delta}(1-\textstyle\sum\beta-\sum\beta'-\sum\gamma)(\beta_1+\beta_2)^{-1}(\beta_1'+\beta_2')^{-1}\Lambda_0^{6}(D_0+i\epsilon)^{-7+\zeta}\,|$$
$$\times |D^0_{1490,1690}|\,\{\lambda[A_1\bar{\alpha}_3\alpha_5\bar{\alpha}_3'\alpha_5 + A_2(\beta_1'+\beta_2')^{-1}\bar{\alpha}_3\alpha_5\alpha_4'\alpha_6' + A_3(\beta_1+\beta_2)^{-1}\alpha_4\alpha_6\bar{\alpha}_3'\alpha_5$$
$$+ A_4(\beta_1+\beta_2)^{-1}(\beta_1'+\beta_2')^{-1}\alpha_4\alpha_6\alpha_4'\alpha_6'] + i\epsilon\}^{-2+\zeta}, \tag{F41}$$

where $\Lambda_0$, $D_0$, and $D^0_{1490,1690}$ are respectively $\Lambda$, $D$, and $D_{1490,1690}$ with all $\alpha$ and all $\alpha'$ set to be zero. In (F41),

$$A_1 = \gamma_1(\beta_5+\beta_6)(\beta_5'+\beta_6'),$$
$$A_2 = \beta_7'(\beta_5+\beta_6)(\beta_3'+\beta_4'),$$
$$A_3 = \beta_7(\beta_3+\beta_4)(\beta_5'+\beta_6'), \tag{F42}$$

and

$$A_4 = \gamma_2(\beta_3+\beta_4)(\beta_3'+\beta_4')$$

are all non-negative. Here $\lambda$ is, from (F38), simply

$$\lambda = \text{sign of } \begin{vmatrix} \beta_7+\gamma_1 & \beta_7+\beta_7'+\gamma_1+\gamma_2 \\ -\gamma_1 & -\beta_7'-\gamma_1 \end{vmatrix}$$
$$= \text{sign of } (\gamma_1\gamma_2 - \beta_7\beta_7')$$
$$= \text{sign of } (A_1A_4 - A_2A_3). \tag{F43}$$

In view of (F41), let us take $\lambda = +1$ and consider the following integral

$$J(\zeta) = \int_0^1 d\alpha_3 d\alpha_4 d\alpha_5 d\alpha_6 d\alpha_3' d\alpha_4' d\alpha_5' d\alpha_6' (A_1\alpha_3\alpha_5\alpha_3'\alpha_5' + A_2\alpha_3\alpha_5\alpha_4'\alpha_6' + A_3\alpha_4\alpha_6\alpha_3'\alpha_5' + A_4\alpha_4\alpha_6\alpha_4'\alpha_6')^{-2+\zeta} \tag{F44}$$

when $\zeta$ is a small positive number. If we scale with respect to the pairs $(\alpha_3, \alpha_4)$, $(\alpha_5, \alpha_6)$, $(\alpha_3', \alpha_4')$, and $(\alpha_5', \alpha_6')$, then

$$J(\zeta)=\zeta^{-4}\int_0^1 d\alpha_3 d\alpha_4 d\alpha_5 d\alpha_6 d\alpha_3' d\alpha_4' d\alpha_5' d\alpha_6' \,\delta(1-\alpha_3-\alpha_4)\delta(1-\alpha_5-\alpha_6)\delta(1-\alpha_3'-\alpha_4')\delta(1-\alpha_5'-\alpha_6')$$
$$\times(A_1\alpha_3\alpha_5\alpha_3'\alpha_5'+A_2\alpha_3\alpha_5\alpha_4'\alpha_6'+A_3\alpha_4\alpha_6\alpha_3'\alpha_5'+A_2\alpha_4\alpha_6\alpha_4'\alpha_6')^{-2+\zeta}\,. \tag{F45}$$

We can still scale with respect to the pairs $(\alpha_3, \alpha_6)$ or $(\alpha_4, \alpha_5)$, and $(\alpha_3', \alpha_6')$ or $(\alpha_4', \alpha_5')$. These four regions are all the same, so we get

$$J(\zeta)\sim\zeta^{-6}\int_0^1 d\alpha_3 d\alpha_6 d\alpha_3' d\alpha_6' \,\delta(1-\alpha_3-\alpha_6)\delta(1-\alpha_3'-\alpha_6')(A_1\alpha_3\alpha_3'+A_2\alpha_3\alpha_6'+A_3\alpha_6\alpha_3'+A_4\alpha_6\alpha_6')^{-2+\zeta}$$
$$\sim\zeta^{-6}\int_0^1 d\alpha_3 d\alpha_3'[A_4+(A_2-A_4)\alpha_3+(A_3-A_4)\alpha_3'+(A_1-A_2-A_3+A_4)\alpha_3\alpha_3']^{-2}$$
$$=\zeta^{-6}(A_1A_4-A_2A_3)^{-1}\ln[(A_1A_4)/(A_2A_3)]\,. \tag{F46}$$

Finally the substitution of (F46) into (F39) yields

$$I_{1,1}^{(20)}(\zeta)\sim-\tfrac{1}{252}\pi i\zeta^{-8}\int d\beta d\beta' d\gamma\,\delta(1-\textstyle\sum\beta-\sum\beta'-\sum\gamma)\Lambda_0^{\,6}D_0^{-7}\,|\ln(\gamma_1\gamma_2)-\ln(\beta_7\beta_7')|\,, \tag{F47}$$

and hence

$$I_{1,1}^{(20)}\sim-\frac{1}{7!252}\,\pi i s^{-3}(\ln s)^7$$
$$\times\int d\beta_1\cdots d\beta_7 d\beta_1'\cdots d\beta_7' d\gamma_1 d\gamma_2\,\delta\Big(1-\sum_1^7\beta_i-\sum_1^7\beta_i'-\sum_1^2\gamma_i\Big)\Lambda_0^{\,6}D_0^{-7}\,|\ln(\gamma_1\gamma_2)-\ln(\beta_7\beta_7')|\,. \tag{F48}$$

This is the desired answer for region 1.

The most peculiar feature of this answer is that it cannot be naturally represented in transverse-momentum space. This and other related questions are studied in Appendix G.

## APPENDIX G

In this appendix we discuss the important and interesting problem of summing over the *signature partners* of a diagram. Suppose we are given a four-particle diagram and one of the important regions of contribution, as discussed, for example, after (F7). Draw the diagram such that each of the Feynman parameters that appear in the top and bottom lines is small. The signature partners are defined to be those three diagrams, together with their respective important regions of contributions, that differ from the original diagram only in that the connections to the middle segment of the top and/or the bottom line are reversed. This is best illustrated by an example. Consider the diagram treated in Appendix F with its first region of contribution; then we obtain from Fig. 10 the three signature partners as shown in Figs. 11–13. In relation to the $I_{1,1}^{(20)}$ of Appendix F, let the corresponding contributions be $I_{1,1t}^{(20)}$, $I_{1,1t'}^{(20)}$, and $I_{1,1tt'}^{(20)}$, where $t$ and $t'$ designate transposing lines respectively in the top and bottom lines of the diagram. We are interested in the sum

$$I_{1,1s}^{(20)}=I_{1,1}^{(20)}+I_{1,1t}^{(20)}+I_{1,1t'}^{(20)}+I_{1,1tt'}^{(20)}\,. \tag{G1}$$

Let us first compare Fig. 10 with Fig. 11. If we write down a $10\times10$ matrix for the diagram of Fig. 11 in a way similar to (F3), the result differs from (F3) in the following ways: First, the (2, 10) element is $-\alpha_3$ instead of $\alpha_3$; secondly, the (1, 2) element is also $-\alpha_3$ instead of $\alpha_3$; thirdly, the (4, 10) element is $\alpha_1+\alpha_3$ instead of $\alpha_1$; fourthly, the (4, 4) element has an additional $+\alpha_3$; fifthly, the (1, 4) element has an additional $+\alpha_3$; and finally, the (2, 4) and (4, 2) elements both have an additional $-\alpha_3$. Let us recall at this point that for this first region of contribution, the variable $\alpha_3$ is scaled twice; first with $\alpha_1$ and $\alpha_2$ as given by (F31), and again with $\alpha_4$ in the evaluation of $J(\zeta)$ defined by (F44). Therefore an additional $\alpha_3$ reduces the size of the integral by at least a factor of $(\ln s)^2$. For this reason, a reference to (F15) shows that only the first difference listed above is significant. Therefore, the effect of transposing lines at the top of the diagrams is to change the sign of $\alpha_3$. Similarly, the effect of transposing at the bottom is to change the sign of $\alpha_3'$.

In order to get the high-energy behavior of $I_{1,1t}^{(20)}$, $I_{1,1t'}^{(20)}$, and $I_{1,1tt'}^{(20)}$ from $I_{1,1}^{(20)}$, we need only to replace the $J(\zeta)$ of (F44) by, respectively,

$$J_t(\zeta)=\int_0^1 d\alpha_3 d\alpha_4 d\alpha_5 d\alpha_6 d\alpha_3' d\alpha_4' d\alpha_5' d\alpha_6' (-A_1\alpha_3\alpha_5\alpha_3'\alpha_5'-A_2\alpha_3\alpha_5\alpha_4'\alpha_6'+A_3\alpha_4\alpha_6\alpha_3'\alpha_5'+A_4\alpha_4\alpha_6\alpha_4'\alpha_6'+i\epsilon)^{-2+\zeta}, \tag{G2}$$

$$J_{t'}(\zeta)=\int_0^1 d\alpha_3 d\alpha_4 d\alpha_5 d\alpha_6 d\alpha_3' d\alpha_4' d\alpha_5' d\alpha_6' (-A_1\alpha_3\alpha_5\alpha_3'\alpha_5'+A_2\alpha_3\alpha_5\alpha_4'\alpha_6'-A_3\alpha_4\alpha_6\alpha_3'\alpha_5'+A_4\alpha_4\alpha_6\alpha_4'\alpha_6'+i\epsilon)^{-2+\zeta}, \tag{G3}$$

and

$$J_{tt'}(\zeta)=\int_0^1 d\alpha_3 d\alpha_4 d\alpha_5 d\alpha_6 d\alpha_3' d\alpha_4' d\alpha_5' d\alpha_6' (A_1\alpha_3\alpha_5\alpha_3'\alpha_5'-A_2\alpha_3\alpha_5\alpha_4'\alpha_6'-A_3\alpha_4\alpha_6\alpha_3'\alpha_5'+A_4\alpha_4\alpha_6\alpha_4'\alpha_6'+i\epsilon)^{-2+\zeta}. \tag{G4}$$

But these three integrals can be evaluated by continuing analytically (F46) in the $A$ coefficients, and the results are

$$J_t(\zeta)\sim\zeta^{-6}(-A_1A_4+A_2A_3)^{-1}\ln[(A_1A_4)/(A_2A_3)]$$
$$\sim -J(\zeta), \tag{G5}$$

$$J_t(\zeta)\sim\zeta^{-6}(-A_1A_4+A_2A_3)^{-1}\ln[(A_1A_4)/(A_2A_3)]$$
$$\sim -J(\zeta), \tag{G6}$$

and

$$J_{tt'}(\zeta)\sim\zeta^{-6}(A_1A_4-A_2A_3)^{-1}\ln\{(A_1A_4)/[(-A_2+i\epsilon)(-A_3+i\epsilon)]\}=J(\zeta)-2\pi i\zeta^{-6}(A_1A_4-A_2A_3)^{-1}. \tag{G7}$$

The sum is thus

$$J_s(\zeta)=J(\zeta)+J_t(\zeta)+J_{t'}(\zeta)+J_{tt'}(\zeta)\sim -2\pi i\zeta^{-6}(A_1A_4-A_2A_3)^{-1}. \tag{G8}$$

Note that the right-hand of (G8) is purely imaginary while the right-hand side of (F46) is purely real. Since this $i$ changes into $-i$ by complex conjugation when $\lambda$ changes sign, we get finally

$$I^{(20)}_{1,1s}(\zeta)\sim -\tfrac{1}{126}\pi^2\zeta^{-8}\int_0^1 d\beta d\beta' d\gamma\delta(1-\textstyle\sum\beta-\sum\beta'-\sum\gamma)\Lambda_0^6(D_0+i\epsilon)^{-7-\zeta} \tag{G9}$$

and

$$I^{(20)}_{1,1s}(s)\sim -\frac{1}{7!126}\pi^2 s^{-3}(\ln s-i\pi)^7\int_0^1 d\beta d\beta' d\gamma\delta(1-\textstyle\sum\beta-\sum\beta'-\sum\gamma)\Lambda_0^6 D_0^{-7}. \tag{G10}$$

The sum over signature partners is thus much nicer and can be easily expressed as an integral in transverse-momentum space. Note that both (F48) and (G10) are of the order $s^{-3}(\ln s)^7$.

Corresponding sums over signature partners for the regions 2, 3, and 4 as discussed after (F7) are exactly the same. The signature partners, however, do not come from the same diagrams.

---

*Work supported in part by the U. S. Atomic Energy Commission under Contract No. AT(11-1)-3227.

†Alfred P. Sloan Fellow.

‡Permanent address: Harvard University, Cambridge, Massachusetts 02138.

§Operated by Universities Research Association, Inc. under contract with the United States Atomic Energy Commission.

[1]S. Mandelstam, Nuovo Cimento 30, 1113 (1963); 30, 1127 (1963); 30, 1143 (1963).

[2]J. C. Polkinghorne, J. Math. Phys. 4, 1396 (1963).

[3]J. C. Polkinghorne, Phys. Lett. 7, 217 (1963).

[4]J. C. Polkinghorne, J. Math. Phys. 6, 1960 (1965).

[5]D. I. Olive, Nuovo Cimento 37, 1422 (1965).

[6]V. N. Gribov, I. Ya. Pomeranchuk, and K. A. Ter-Martirosyan, Yad Fiz. 2, 361 (1966) [Sov. J. Nucl. Phys. 2, 258 (1966)]; Phys. Rev. 139, B184 (1965).

[7]P. Osborne and J. C. Polkinghorne, Nuovo Cimento 47, 522 (1967).

[8]D. I. Olive and J. C. Polkinghorne, Phys. Rev. 171, 1475 (1968).

[9]V. N. Gribov, Zh. Eksp. Teor. Fiz. 53, 654 (1968) [Sov. Phys.—JETP 26, 414 (1968)].

[10]J. C. Polkinghorne, Nuovo Cimento 56A, 755 (1968).

[11]V. N. Gribov and A. A. Migdal, Zh. Eksp. Teor. Fiz. 55, 1498 (1969) [Sov. Phys.—JETP 28, 784 (1969)];

Yad. Fiz. 8, 1002 (1968) [Sov. J. Nucl. Phys. 8, 583 (1969)]; *ibid.* 8, 1213 (1969) [*ibid.* 8, 703 (1969)].
[12]J. C. Polkinghorne, Nucl. Phys. B6, 441 (1969).
[13]J. B. Bronzan, Phys. Rev. D 4, 1097 (1971).
[14]P. Goddard and A. R. White, Nuovo Cimento 1A, 645 (1971).
[15]V. N. Gribov, E. M. Levin, and A. A. Migdal, Yad. Fiz. 12, 173 (1970) [Sov. J. Nucl. Phys. 12, 93 (1971)].
[16]A. R. White, Nucl. Phys. B39, 432 (1972); B39, 461 (1972).
[17]A. R. White, Nucl. Phys. B50, 93 (1972); B50, 130 (1972).
[18]J. L. Cardy and A. R. White, Phys. Lett. 47B, 445 (1973).
[19]H. D. I. Abarbanel and J. B. Bronzan, Phys. Rev. D 9, 2397 (1974); 9, 3304 (1974).
[20]H. D. I. Abarbanel and J. B. Bronzan, Phys. Lett. 48B, 345 (1974); A. A. Migdal, A. M. Polyakov, and K. T. Ter-Martirosyan, *ibid.* 48B, 239 (1974).
[21]D. Amati, S. Fubini, and A. Stanghellini, Phys. Lett. 1, 29 (1962); D. Amati, A. Stanghellini, and S. Fubini, Nuovo Cimento 26, 896 (1962).
[22]The diagram of Fig. 2(c) has been previously considered by Polkinghorne in Ref. 3, but his calculation is not quite accurate enough for our purposes.
[23]A related class of diagrams which does not include our conditions (2) and (4) has been studied in a multiperipheral model by S. Auerbach, R. Aviv, R. Sugar, and R. Blankenbecler [Phys. Rev. Lett. 29, 522 (1972); Phys. Rev. D 6, 2216 (1972)]. See, however, A. Swift, Nucl. Phys. B84, 397 (1975). For a different model see R. Blankenbecler and H. M. Fried, Phys. Rev. D 8, 678 (1973).
[24]G. M. Cicuta and R. L. Sugar, Phys. Rev. D 3, 970 (1971).
[25]B. Hasslacher and D. K. Sinclair, Phys. Rev. D 3, 1770 (1971).
[26]K. Symanzik, Prog. Theor. Phys. 20, 690 (1958).
[27]J. S. R. Chisolm, Proc. Camb. Philos. Soc. 48, 300 (1952).
[28]J. D. Bjorken and T. T. Wu, Phys. Rev. 130, 2566 (1963).
[29]See for example A. C. Aitken, *Determinants and Matrices* (Interscience, New York, 1951), p. 99.